EUROPEAN ORGANIZATION FOR NUCLEAR RESEARCH

CERN-EP/85-36
18 March 1985

ELASTIC SCATTERING AND TOTAL CROSS-SECTION AT VERY HIGH ENERGIES

Rino Castaldi[1] and Giulio Sanguinetti[1]

INFN, Sezione di Pisa, Italy

To be published in

Annual Review of Nuclear and Particle Science

---

1) Visitors at CERN, Geneva, Switzerland

CONTENTS

1. INTRODUCTION

The unexpected rise of the proton-proton total cross-section (1, 2) discovered many years ago, at the beginning of the operation of the CERN Intersecting Storage Rings (ISR), has excited renewed interest in the asymptotic behaviour of hadron interactions. An old common prejudice expects that at very high energies the mechanisms that control hadron scattering become simpler and can be interpreted in terms of a few basic principles, more general than any specific model. Indeed, while at low energy hadron cross-sections show a pattern rich in bumps and structures, at higher energies their behaviour appears to be smooth, suggesting that the laws of strong interactions become simpler and merely follow from general assumptions independent of the details of particle dynamics. Such a high-energy limit appears however to be approached very slowly, and a large span in energy is certainly required in order to speculate upon this subject.

The successful cooling technique (3) of antiproton beams at CERN has recently allowed the acceleration of proton and antiproton bunches simultaneously circulating in opposite directions in the Super Proton Synchrotron (SPS). Hadron-hadron collisions could so be produced at a centre-of-mass energy one order of magnitude higher than previously available, thus opening a new wide range of energies to experimentation. This technique also made it possible to replace one of the two proton beams in the ISR by a beam of antiprotons, allowing a direct precise comparison, by the same detectors, of pp and $\bar{p}p$ processes at the same energies.

The aim of this review is to summarize the recent progress in the field of elastic scattering and total cross-section in this new energy domain. In Section 2 a survey of the experimental situation is outlined.

The most significant data are presented with some emphasis on the interpretation, without going into specific details or technicalities. This section is therefore intended to give a self-contained outlook of the field, having in mind also the non-specialized reader. In Section 3 hadron scattering at high energy is described in an impact parameter picture, which provides a model-independent intuitive geometrical representation. The diffractive character of elastic scattering, seen as the shadow of inelastic absorption, is presented as a consequence of unitarity in the s-channel. Spins are neglected throughout this review, inasmuch as the asymptotic behaviour in the very high-energy limit is the main concern here. In Section 4 some relevant theorems are recalled on the limiting behaviour of hadron-scattering amplitudes at infinite energy. There is also a brief discussion on how asymptotically rising total cross-sections imply scaling properties in the elastic differential cross-sections. A quick survey of eikonal models is presented and their predictions are compared with ISR and SPS Collider data.

We apologize that space does not allow us to cover comprehensively this wide subject. In particular, we have preferred to discuss the general aspects of this field rather than to enter into the details of the many current phenomenological models that will not be considered in this article. Furthermore, we have not tried to give exhaustive references and we apologize to those authors whose contributions have not been mentioned. Many excellent reviews on hadron scattering at high energies can be found in the literature. A sample of the most recent ones is listed in Reference (4) for the convenience of the interested reader.

2. REVIEW OF THE EXPERIMENTAL DATA: A GENERAL OUTLOOK OF THE FIELD

2.1 Elastic Scattering

At very high energy, hadron elastic scattering is believed to be well described by a single scalar, mainly imaginary, amplitude and one usually assumes that, as energy increases, spin tends to play a negligible role (see Section 2.2). The interaction becomes mostly absorptive, dominated by the many open inelastic channels. Elastic scattering is then essentially the shadow of the inelastic cross-section. Therefore the elastic amplitude has a mainly diffractive character, in close analogy with the diffraction of a plane wave in classical optics, and its dependence on the momentum transfer t is the Fourier transform of the spatial distribution of the hadronic matter inside the interacting particle. In the simple case of an absorbing disc of radius R and uniform greyness $\xi \leq 1$, to the inelastic cross-section $\sigma_{inel} = \pi R^2 \xi$ corresponds an elastic hadronic diffraction pattern which is a steep function of tR^2. Its integral σ_{el} is bigger for larger ξ up to a maximum value $\sigma_{el} = \sigma_{inel}$ in the limit of a completely black disc ($\xi = 1$).

The elastic differential cross-section $d\sigma/dt$ measured for pp scattering at the ISR (5) is shown in Figure 1 as a function of the four-momentum transfer t, at five values of the total c.m. energy $\sqrt{s}$. A salient feature of these distributions is the presence of a pronounced narrow peak around the forward direction, which decreases almost exponentially in t by more than six orders of magnitude, down to $-t \approx 1.4$ GeV^2. In a geometrical picture, as we shall see in Section 3.4, such a smooth diffraction pattern over so wide a t-interval indicates that the transverse distribution of matter inside the proton is nearly Gaussian. At larger values of $|t|$, a prominent structure is observed, consisting of a sharp minimum followed by a secondary maximum and by a subsequent

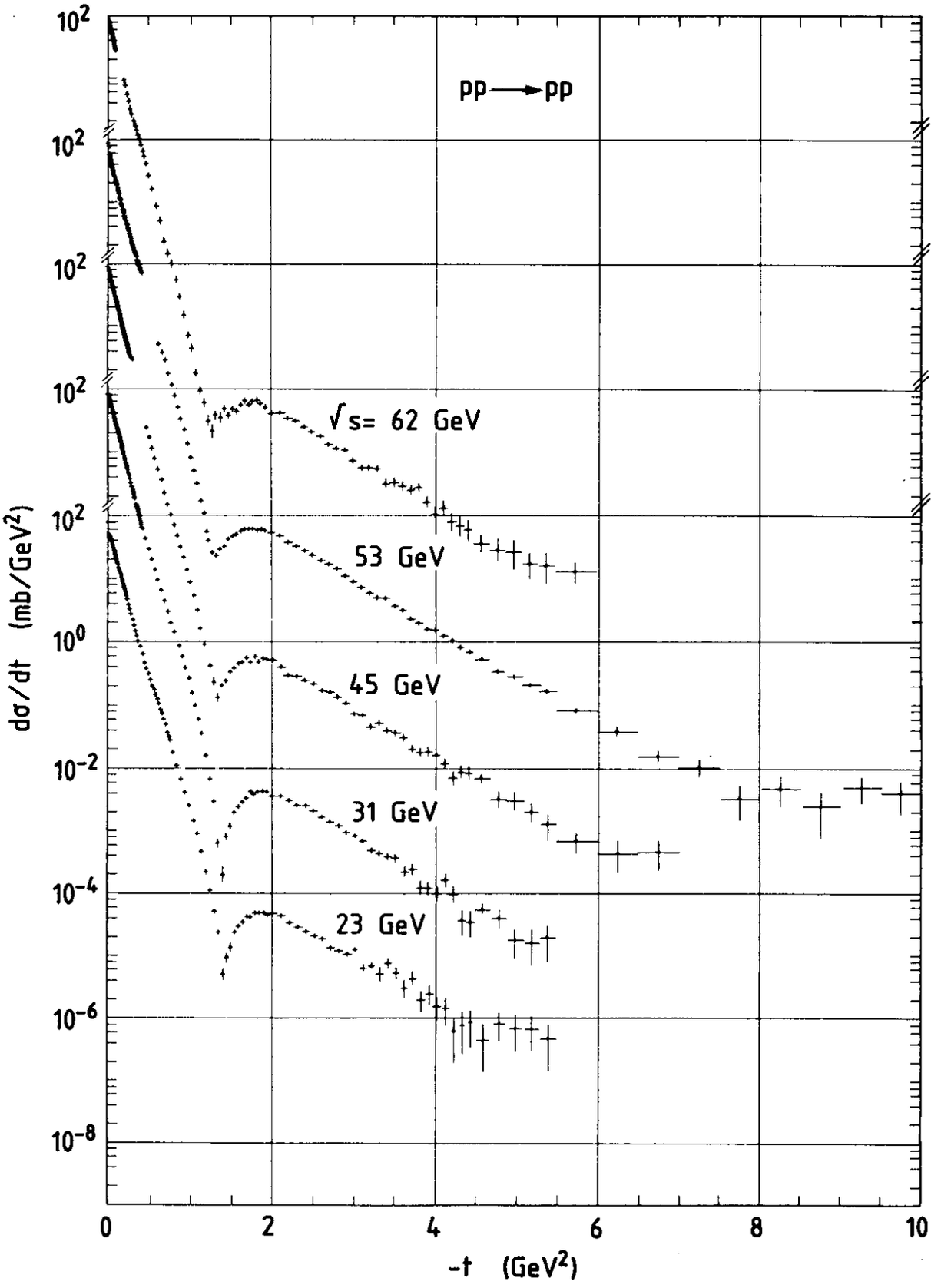

Figure 1. Differential cross-section for pp elastic scattering at the five ISR energies [from Reference (5)].

exponential fall-off by three more orders of magnitude with a much lower slope. As energy increases, the slope of the forward peak becomes steeper and the dip moves towards smaller values of $|t|$. Following the optical analogy, this shrinkage of the diffraction peak indicates an expansion of the interaction radius. A closer look at the diffraction peak reveals a slight variation of slope presumably localized around $-t \approx 0.13$ GeV^2.

In the very forward direction ($-t < 10^{-3}$ GeV^2) the elastic differential cross-section is dominated by the almost real Coulomb amplitude, which is well understood theoretically and can easily be calculated. In the $|t|$ region between 10^{-3} and 10^{-2} GeV^2 the Coulomb and the nuclear amplitude are of the same order of magnitude and may give rise to a non-negligible interference effect, if the hadronic amplitude is not purely imaginary. The measurement of the interference term allows the determination of the phase of the nuclear amplitude F in the forward direction, which is usually expressed as the ratio of the real to the imaginary part of the amplitude at $t = 0$: $\varrho(s) = [\mathrm{Re}\ F(s,t)/\mathrm{Im}\ F(s,t)]_{t=0}$.

2.1.1 THE REGION OF COULOMB-NUCLEAR INTERFERENCE ($0.001 < -t < 0.01$ GeV^2)

In this t-region the elastic differential cross-section is determined by both the nuclear and the Coulomb amplitude: $d\sigma/dt = |f_N \pm f_C \exp[i\varphi(t)]|^2$, where the upper sign is used for pp and the lower sign for $\bar{p}p$ scattering. The nuclear amplitude f_N can be parametrized in terms of the total cross-section σ_{tot} and of the slope B of the forward elastic peak, by means of the optical theorem (see Section 3.2), as $f_N = (1/4\sqrt{\pi})(i + \varrho)\sigma_{tot} \exp(Bt/2)$, disregarding spin effects and assuming that the real and imaginary parts have the same exponential t-dependence in this region. The Coulomb amplitude f_C represents the well-known Rutherford scattering and is expressed by $f_C = -2\sqrt{\pi}\alpha G^2(t)/|t|$, where α is the fine structure constant

and G(t) is the proton electromagnetic form factor. The small phase factor $\varphi(t)$ arises from the simultaneous presence of both hadronic and electromagnetic exchanges in the same diagram (6) and has opposite sign in the pp and the $\bar{p}p$ channels. The relative importance of the interference term is maximum when the nuclear and the Coulomb amplitudes are comparable (at $-t \approx 8\pi\alpha/\sigma_{tot}$). Its contribution to the cross-section in a first approximation is $\approx -(\pm)(\rho + \varphi)\alpha\sigma_{tot}/|t|$ and can easily be distinguished from the steeper $1/t^2$ dependence of the Coulomb term and from the relatively flat nuclear contribution. If the factor $(\rho + \varphi)$ is positive the interference is destructive for pp and constructive for $\bar{p}p$ scattering.

A sizeable destructive interference, which becomes more and more pronounced as energy increases, is indeed observed in the ISR pp data (7) shown in Figure 2. This is the experimental evidence that ρ, which was observed to go through zero at Fermilab energies (8), increases towards

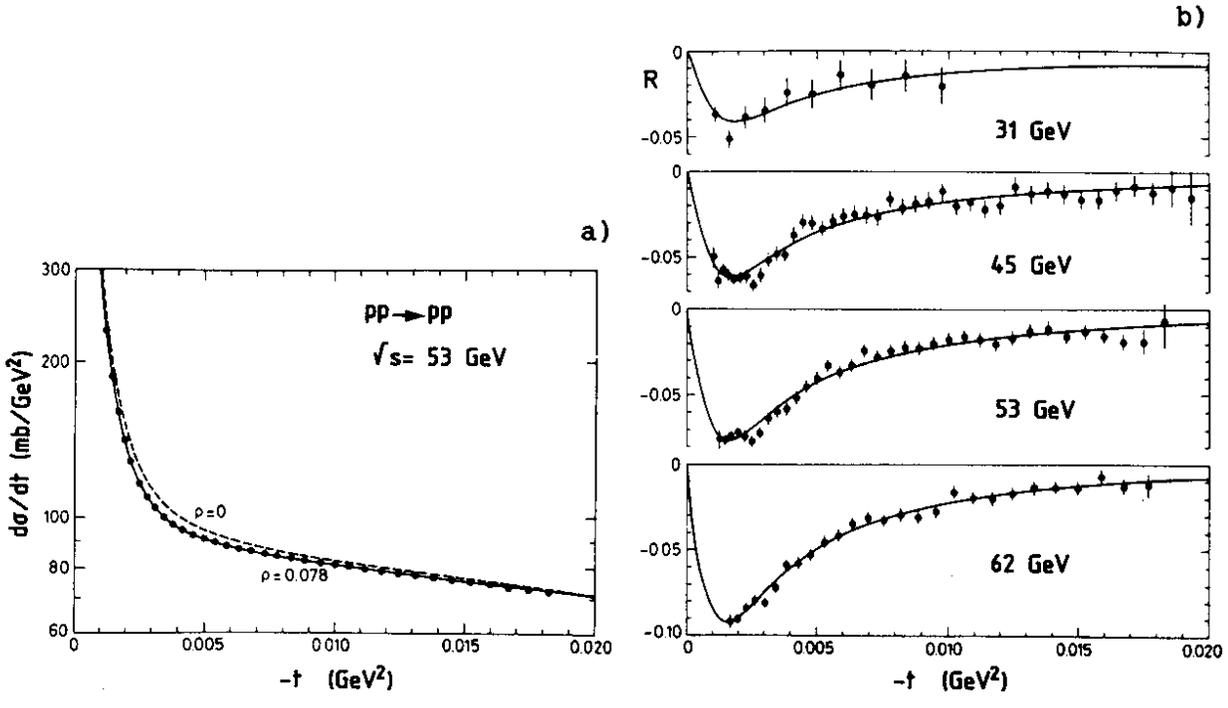

Figure 2. (a) Differential cross-section for pp elastic scattering in the Coulomb region at $\sqrt{s}$ = 53 GeV (the ρ = 0 curve is shown for comparison); (b) destructive interference observed at four ISR energies; R is defined as (dσ/dt measured)/(dσ/dt for ρ = 0) - 1. Data from Reference (7).

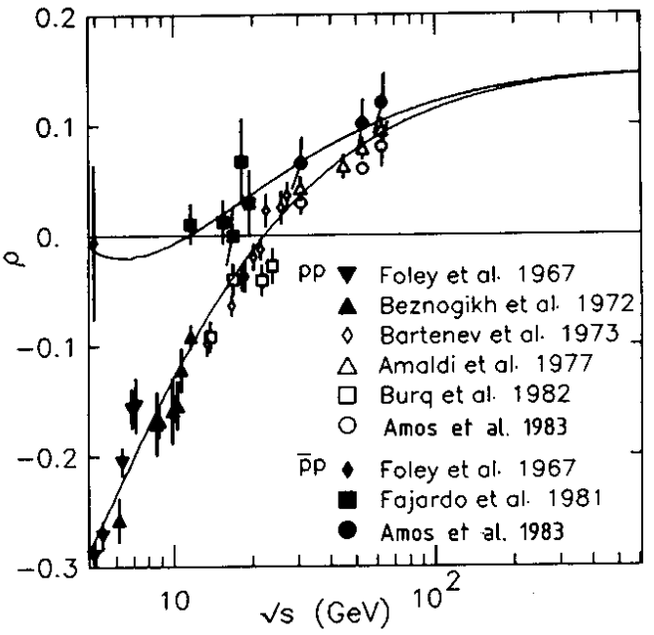

Figure 3. Summary of high-energy data on the real part ϱ for pp and $\bar{p}p$ forward elastic scattering; the curve represents the dispersion relation fit of Reference (7). Figure from Reference (9).

higher and higher positive values over the whole ISR energy range. Data on the $\bar{p}p$ elastic differential cross-section in this t-region have also become available recently at the ISR (9). In this case a constructive interference is observed, which indicates a rising positive value of ϱ in this energy range for $\bar{p}p$ scattering too. A summary of ISR data on ϱ for both pp and $\bar{p}p$ scattering is shown in Figure 3, together with lower energy data.

The real part of the elastic amplitude is related to the imaginary part via dispersion relations. On the other hand, the imaginary part at t = 0 is related to the total cross-section by the optical theorem. As a consequence, it is possible to write the parameter ϱ at a given energy as an integral of the total cross-section over energy. Such an integral relation can be approximated by a local expression which relates ϱ to the derivative of σ_{tot} with respect to energy (10, 11):

$$\varrho(s) \approx (\pi/2\sigma_{tot})\, d\sigma_{tot}/d \ln s \ . \qquad 1.$$

Equation 1 is not really adequate to compute the values of ϱ as a function of energy in a quantitative way but has the merit of describing the qualitative connection between ϱ and σ_{tot} at asymptotic energies in a transparent way. In particular, it allows one to understand easily the result, rigorously proved in Reference (12), that a rising total cross-section implies a positive value of ϱ. For instance, in the case of an asymptotic behaviour which saturates the Froissart bound ($\sigma_{tot} \sim \ln^2 s$), ϱ goes to zero from positive values as $\pi/\ln s$.

2.1.2 THE DIFFRACTION PEAK REGION ($0.01 < -t < 0.5$ GeV^2) Recent data on $\bar{p}p$ elastic scattering at the ISR are compared in Figure 4 with pp data

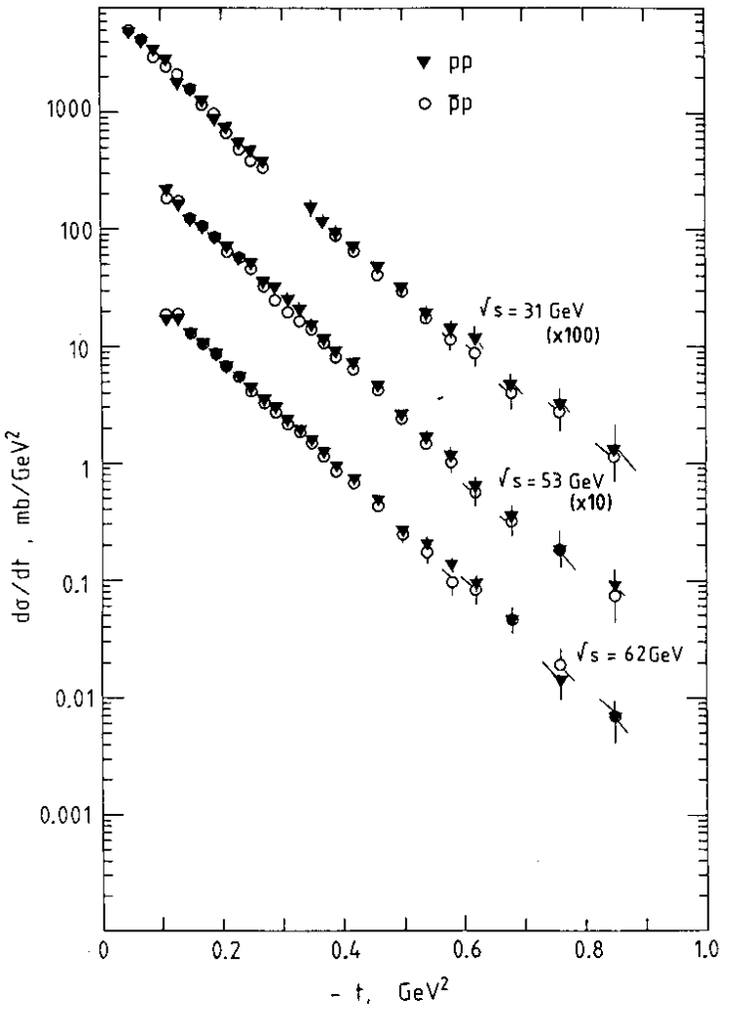

Figure 4. Comparison of pp and $\bar{p}p$ diffraction peaks at three ISR energies, [from Reference (13a)].

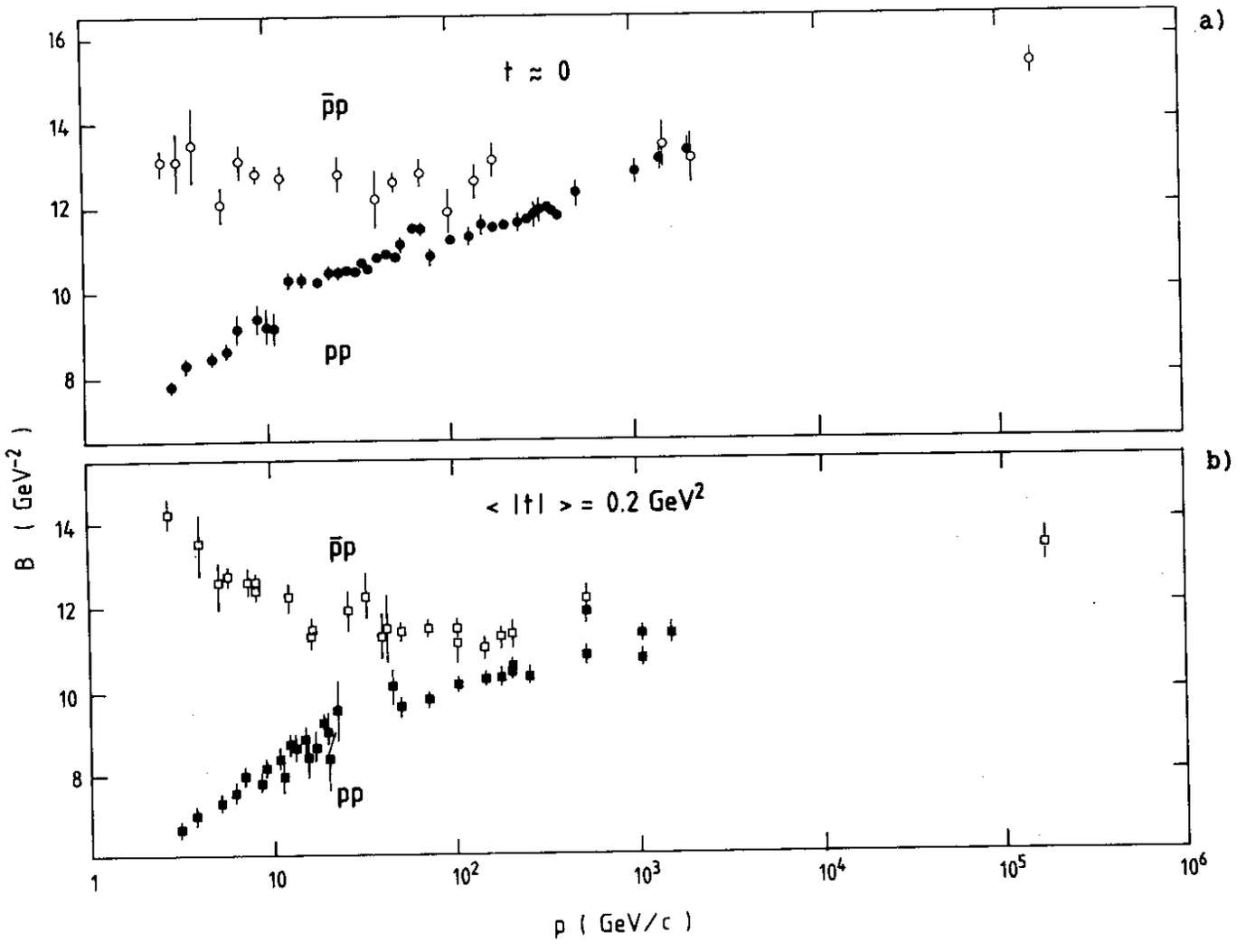

Figure 5. A compilation of slopes of pp and $\bar{p}p$ diffraction peaks (black points and open points, respectively) as a function of energy; (a) in the forward direction [early, low-statistics measurements at the SPS Collider (17, 18) have not been included]; (b) around $-t \approx 0.2$ GeV^2 [from References (13a, 14a)].

taken at the same energies by the same experiment (13a). It is remarkable how the shape of the $\bar{p}p$ distribution, which is notably steeper at lower energies, becomes similar to that of pp distribution in the ISR energy range. The energy dependence of the slope of the elastic differential cross-section for $\bar{p}p$ and pp scattering, shown in Figure 5, indicates a shrinkage of the diffraction peak at a rate of at least ln s (14). It appears evident from there that, as energy increases, the antiproton and the proton tend to behave exactly in the same way. Such a behaviour is indeed expected at asymptotic energies, since the Cornille-Martin theorem (see Section 4.1.3) states that the elastic differential cross-sections of particle and antiparticle in the region of the diffraction peak tend to be the same for $s \to \infty$.

From Figure 5 one can also notice that the value of the slope B is different at different values of t. As a matter of fact, the forward elastic peak deviates from a pure exponential in t, and rather than a constant slope B one should introduce a local slope $B(t) = (d/dt) \ln (d\sigma/dt)$. A slope which continuously decreases with increasing $|t|$ is observed up to Fermilab energies, where the elastic diffraction peak is reasonably well described by an exponential with the addition of a small quadratic term (15), of the kind $\exp (Bt + Ct^2)$. On the other hand, ISR data exhibit a rather sudden break localized around $-t \approx 0.13$ GeV^2. A similar feature is observed in the $\bar{p}p$ elastic differential cross-section measured at the SPS Collider at $\sqrt{s} = 546$ GeV. As illustrated in Figure 6, in the region $0.03 < -t < 0.15$ GeV^2 the data show no hint of curvature and are well fitted by a single exponential (16) of slope $B = 15.2 \pm 0.2$ GeV^{-2} with no need for a quadratic term. A significant quadratic dependence can only be obtained from fits over a t-region that extends up to at least 0.3 GeV^2. However, such a parametrization appears to be inadequate to represent the data in the t-range from 0.03 to

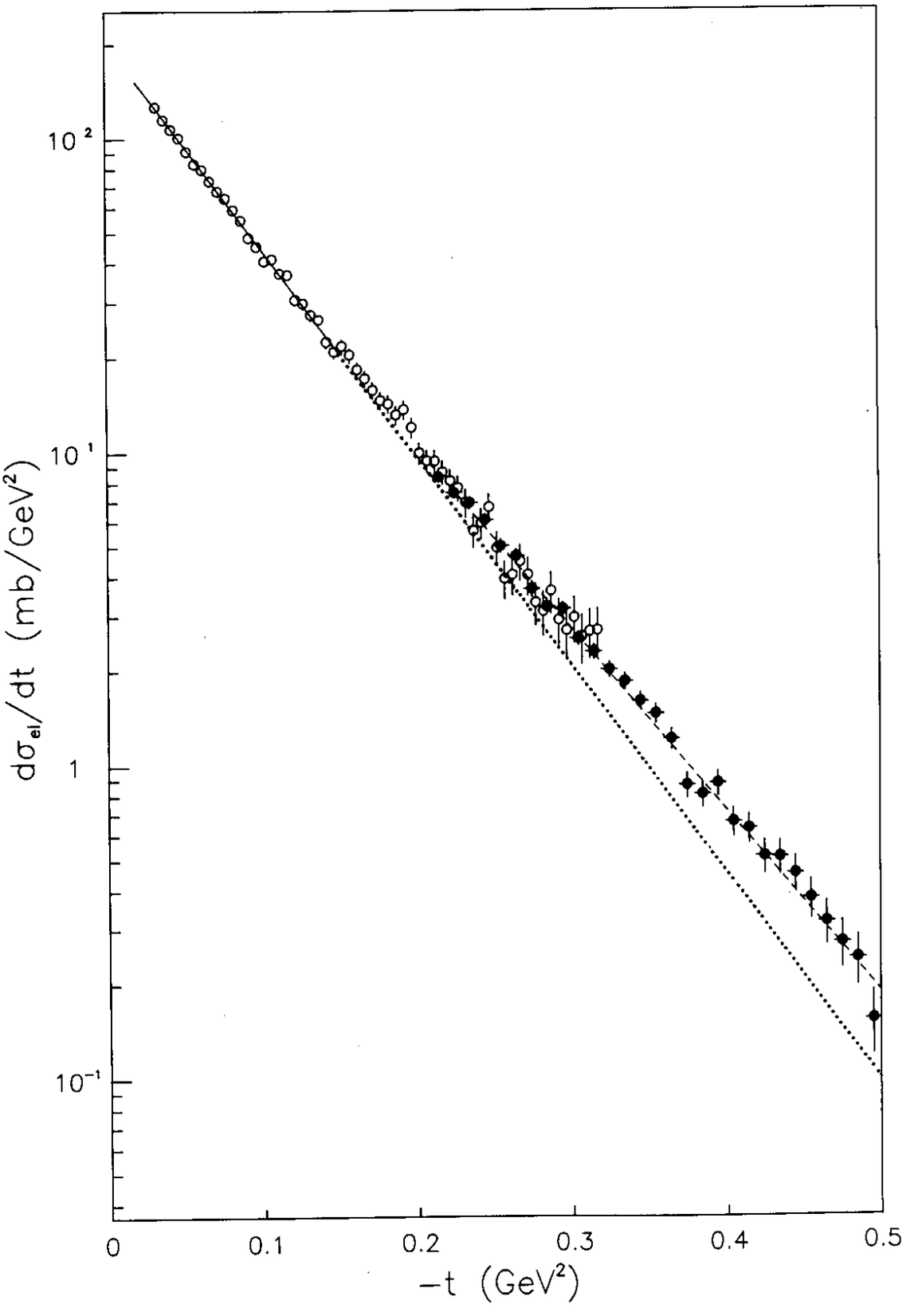

Figure 6. Elastic differential cross-section for $\bar{p}p$ at $\sqrt{s}$ = 546 GeV; the lines are single-exponential fits below and above $-t \approx 0.15$ GeV^2 [from Reference (16)].

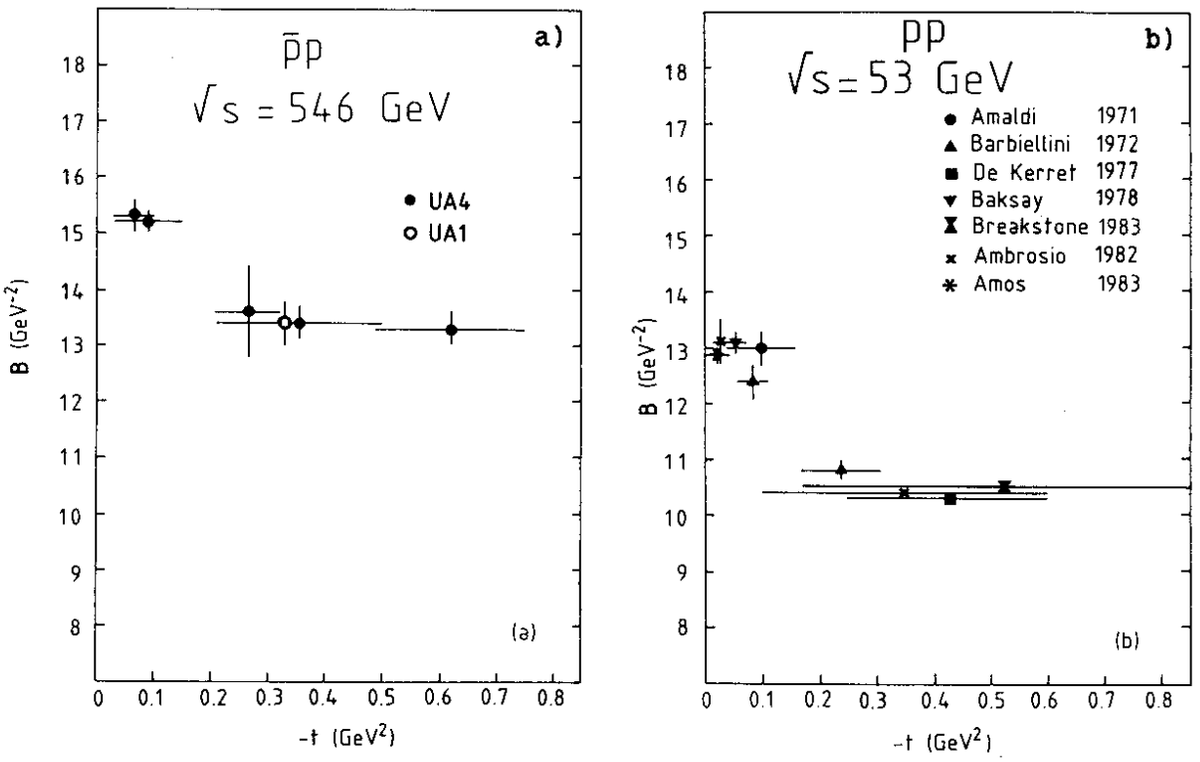

Figure 7. Local slope of the elastic diffraction peak as a function of t [from Reference (20)]: (a) for $\bar{p}p$ at $\sqrt{s}$ = 546 GeV; (b) for pp at $\sqrt{s}$ = 53 GeV. The horizontal bars indicate the t-interval in which the exponential fit was performed.

0.5 GeV^2. On the other hand, a single exponential also fits the data in the region $0.2 < -t < 0.7$ GeV^2: it is remarkable that in such a wide t-interval the slope appears to remain constant (16-19), with a value of 13.4 ± 0.3 GeV^{-2}. The phenomenon of a fast slope variation by about two units in a small t-interval between 0.1 and 0.2 GeV^2 is represented in Figure 7 [from Reference (20)], where the local slope of the diffraction peak is shown in various t-intervals, at $\sqrt{s}$= 53 and 546 GeV. Independently of this double-slope structure, the anti-shrinkage observed in $\bar{p}p$ elastic scattering at lower energy turns now into a shrinkage similar to that of the pp diffraction peak. As discussed in Section 3.4, in a geometrical picture the slope of the diffraction peak is proportional to the square of the mean interaction radius: the shrinkage of the diffraction peak therefore reflects an increase of the dimension of the nucleon.

2.1.3 THE LARGE-t REGION ($-t > 0.5$ GeV^2) The main feature of the pp elastic differential cross-section in this t-range is the progressive development, up to ISR energies, of a sharp dip around $-t \approx 1.4$ GeV^2, as illustrated in Figure 8a. In the ISR energy range the position of the dip is observed to move towards smaller $|t|$ values, while the height of the secondary maximum grows, as already shown in Figure 1. It is natural to relate this behaviour to the rising total cross-section observed in the same energy interval. Indeed the diffraction pattern has to shrink, if the increase of σ_{tot} is at least partially due to an expansion of the proton radius. The geometrical scaling hypothesis actually assumes that the increase of σ_{tot} is only due to the increase of the interaction radius R, while the nucleon opacity remains constant. This implies a scaling property in the elastic differential cross-section as a function of the variable $\tau = t\sigma_{tot}$, which indeed seems to be reasonably verified by the ISR data (21) as shown in Figure 8b. However it can be noticed from Figure 1 that the dip appears to get more pronounced at the lower ISR energies, and gradually fills in with increasing energy. As a consequence, a scaling violation in a limited region near the dip can be seen in Figure 8b. In a simple diffractive picture the imaginary part is assumed to be the dominant scaling component of the elastic amplitude and is supposed to vanish at the position of the dip, where only the small real part contributes to the cross-section. This interpretation is supported by the fact that, as shown in Figure 3, ϱ goes through zero at about the energy at which the dip is sharpest (see Section 4.2).

The $\bar{p}p$ elastic differential cross-section already at an incident beam momentum p_{lab} as low as 30 GeV/c (22) starts to exhibit a pronounced dip around $-t \approx 1.7$ GeV^2. At these low energies $\bar{p}p$ and pp elastic

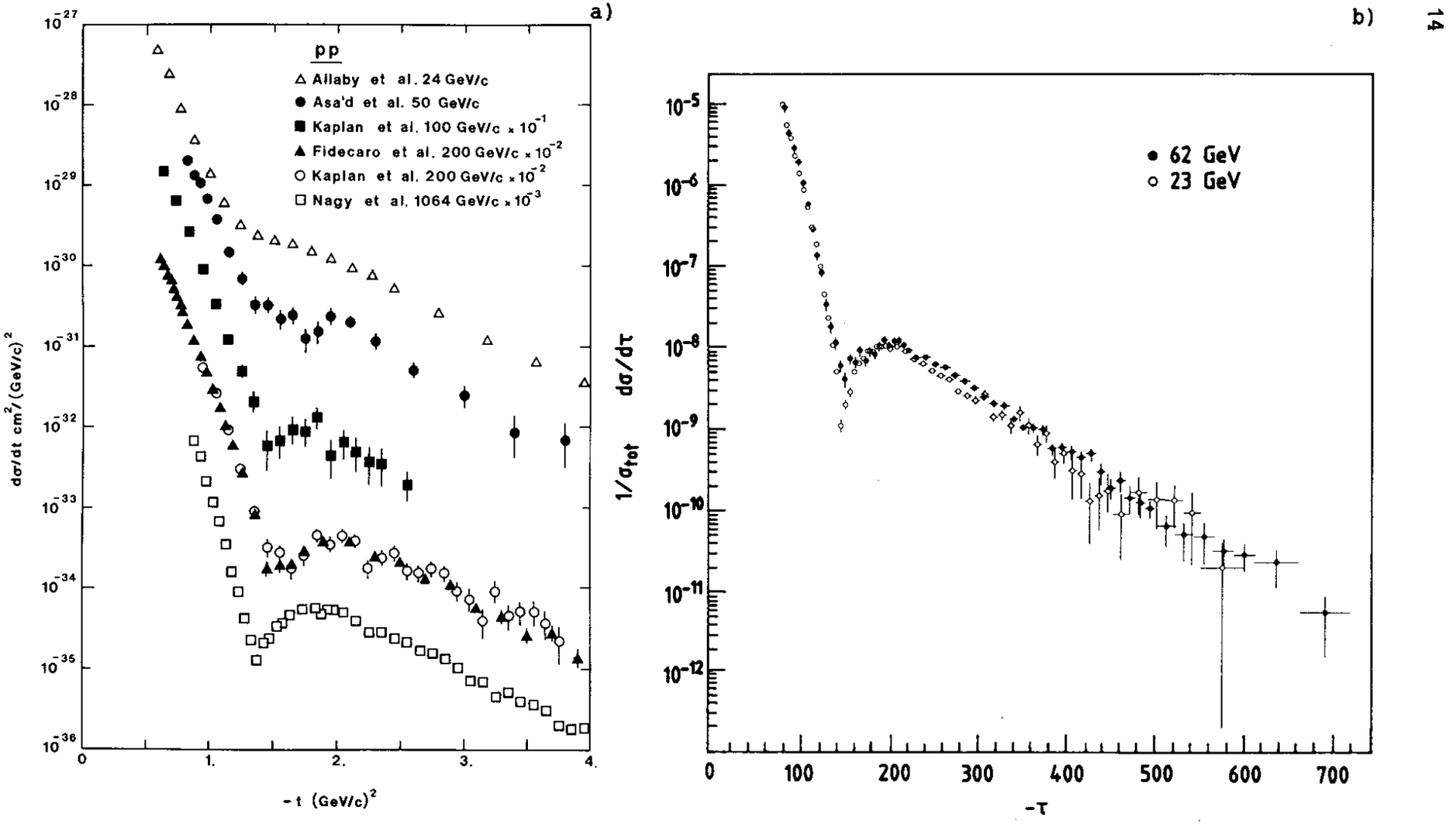

Figure 8. (a) Progressive development of the dip-bump structure in pp elastic differential cross-section from 24 to 1064 GeV/c [from Reference 22)]. (b) Geometrical scaling property of pp elastic differential cross-section in the ISR energy range [from Reference (21)]. The scaling variable τ is expressed in absolute units.

scattering look therefore quite different. A direct comparison is shown in Figure 9a at p_{lab} = 50 GeV/c, where the dip structure in pp scattering is not yet developed. These differences tend to disappear as energy increases. In particular, at p_{lab} = 200 GeV/c there is a well developed pp dip structure around $-t \approx 1.5$ GeV^2, similar to that observed in $\bar{p}p$ scattering at the same energy (23). A direct comparison of $\bar{p}p$ (13b) and pp (21) elastic differential cross-sections at an ISR energy equivalent to p_{lab} = 1500 GeV/c is shown in Figure 9b. Within the limited statistics of the $\bar{p}p$ data, the similarity of the diffraction peaks also extends to the region of the dip, if one considers that the higher value of the real part of the $\bar{p}p$ elastic amplitude at this energy may account for a larger non-diffractive term filling the dip structure more in $\bar{p}p$ than in pp. The possible connection between the depth of the dip and the value of ρ is discussed in detail in Section 4.2. In conclusion, the differences in the $\bar{p}p$ and pp differential cross-sections appear to diminish as energy increases, and it is reasonable to assume that the Cornille-Martin prediction that the two diffraction peaks should become equal is essentially verified beyond ISR energies. Data on $\bar{p}p$ elastic scattering from the SPS Collider at $\sqrt{s}$ = 546 GeV are shown in Figure 10a, compared with ISR pp data at $\sqrt{s}$ = 53 GeV. The conspicuous shrinkage of the diffraction peak is acompanied by a forward movement of the dip structure that now only appears as a simple break of the exponential fall-off at $-t \approx 0.9$ GeV^2. Furthermore, the shoulder observed in $\bar{p}p$ at the Collider is more than one order of magnitude higher than the secondary maximum measured at the ISR.

There are models that attribute the disappearance of the dip in $\bar{p}p$ elastic scattering to an intrinsic difference between the $\bar{p}p$ and the pp channels rather than to the evolution of the diffraction peak as energy

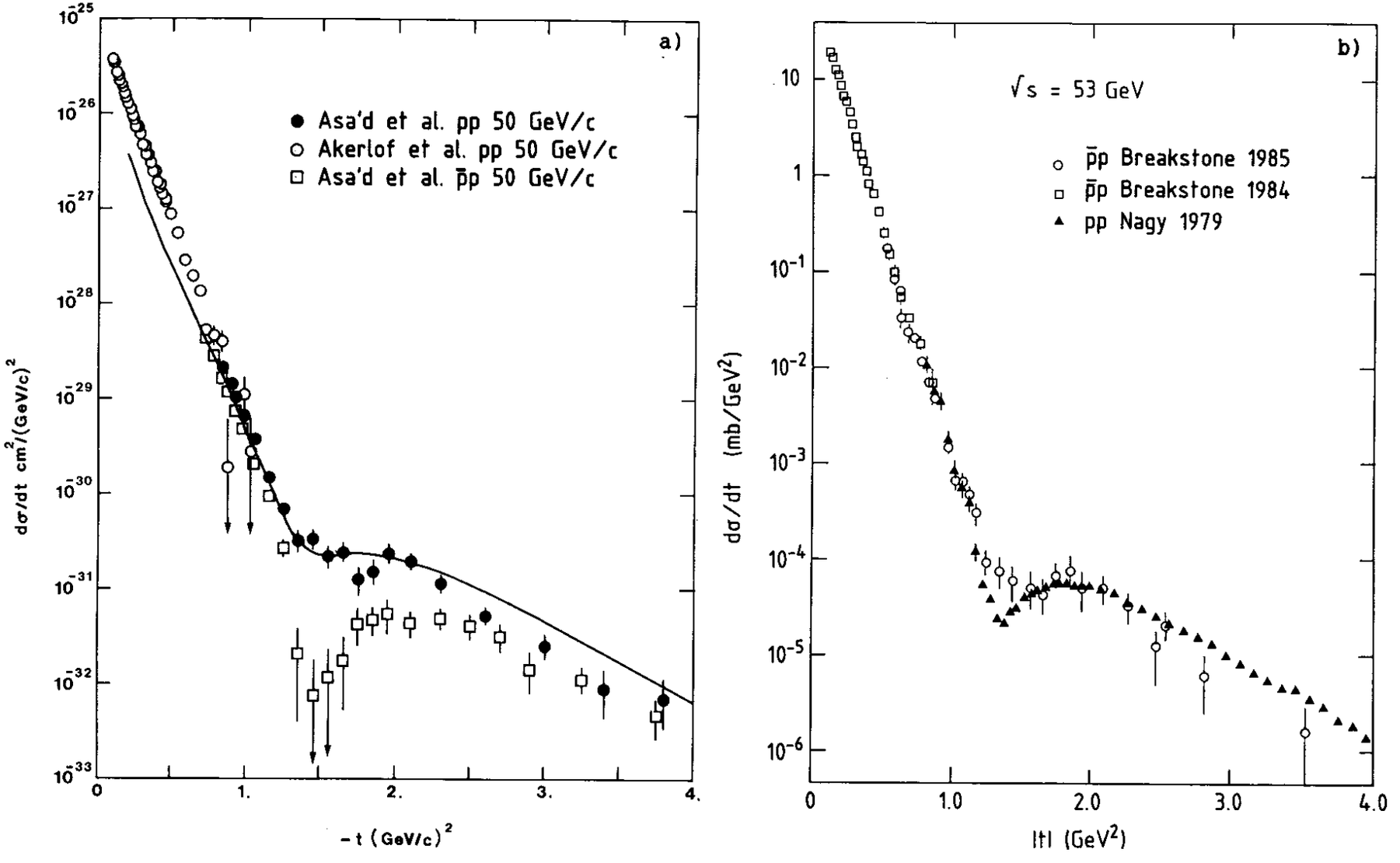

Figure 9. Comparison of the dip-bump structure in pp and $\bar{p}p$ elastic scattering at (a) 50 GeV/c [from Reference (22)], (b) 1500 GeV/c [from Reference (13b)].

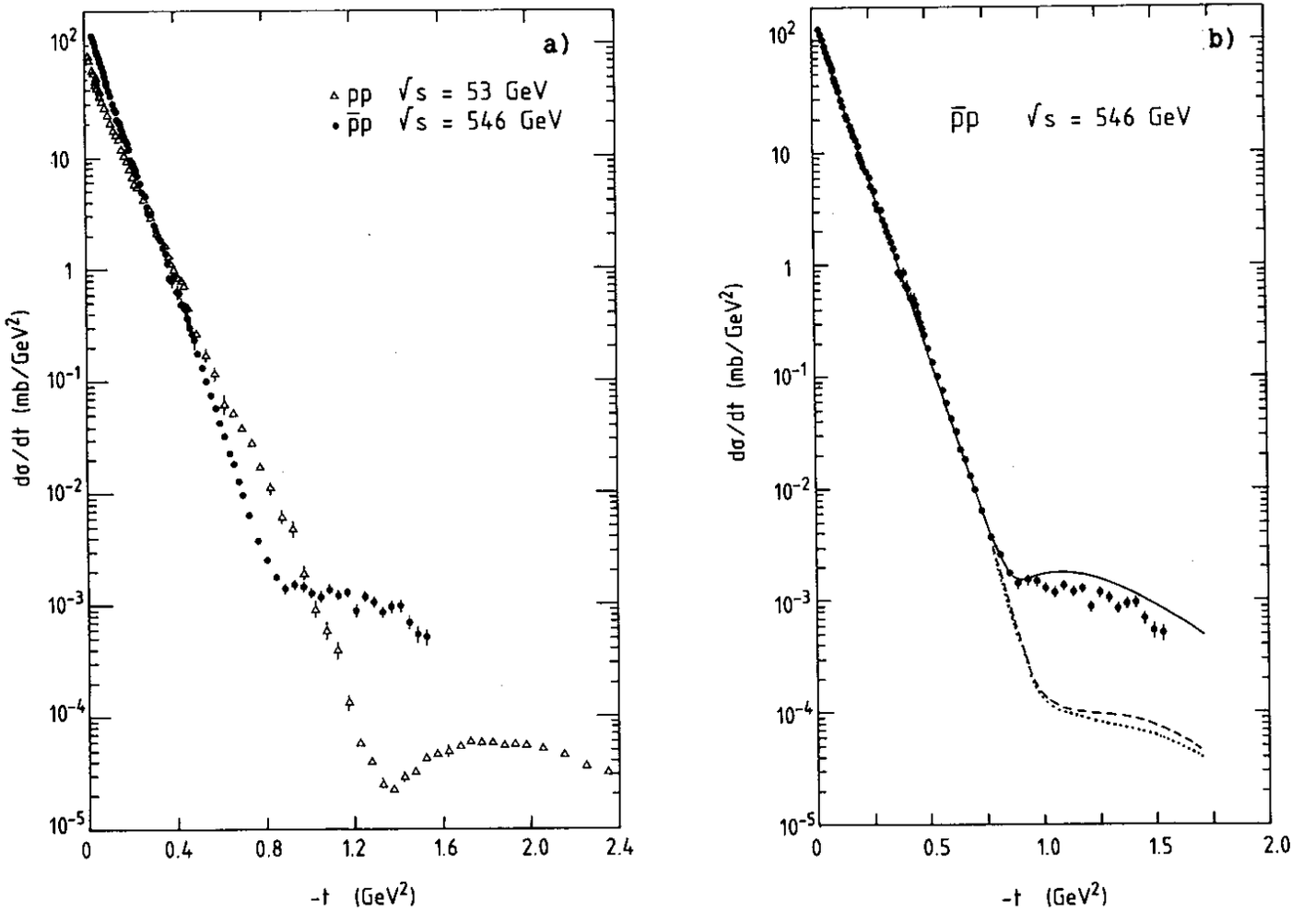

Figure 10. (a) Differential cross-section for $\bar{p}p$ elastic scattering at the CERN SPS Collider at $\sqrt{s}$ = 546 GeV [from Reference (19)]. Data on pp elastic scattering at $\sqrt{s}$ = 53 GeV are also shown. (b) Comparison of different models for $\bar{p}p$ elastic scattering at $\sqrt{s}$ = 546 GeV. Solid line from Reference (28b); dashed line from Reference (24); dotted line from Reference (27). Data from Reference (19).

increases. Indeed QCD diagrams with three-gluon exchanges have been considered (24, 25a), which in principle may give rise to a crossing-odd component in the diffractive peak that can account for a shoulder in $\bar{p}p$ and for a dip in pp at the same time. Good fits can be obtained to ISR pp data, although one might question whether it is plausible to isolate a few QCD diagrams in this t-region. However, the height of the shoulder predicted by this model for $\bar{p}p$ at $\sqrt{s}$ = 546 GeV is about one order of magnitude lower than the SPS Collider data (see dashed line in Figure 10b).

The correct prediction of the height of the shoulder is a serious challenge for all models. Good fits to the large-t structures can be obtained in the 'nucleon core' model (26), but are restricted to this t-region. In the geometrical scaling picture (see Section 4.2), the disappearance of the dip can easily be accounted for by the growing real part of the elastic amplitude (27). In this model, however, the value of the scaled $d\sigma/dt$ grows proportionally to σ_{tot}^2 and is inadequate by one order of magnitude to reproduce the fast growth of the shoulder from ISR to Collider energy (see dotted line in Figure 10b).

A stronger energy dependence of the height of the shoulder is predicted by the eikonal-type models, which can reasonably reproduce ISR and Collider data also in the large-t region (28) (see solid line in Figure 10b). Indeed the prediction of a shoulder at this energy, with about the correct height, ten years before the measurement at the Collider, has to be considered as a remarkable success of factorizing eikonal models, which, as discussed in Section 4.3, are able to reproduce many qualitative features of elastic scattering.

2.2 Total Cross-Section

The total cross-section is one of the basic parameters of hadron-scattering processes. Although this quantity is directly the sum of the many cross-sections of all accessible final states, it is simply related via the optical theorem to the imaginary part of the amplitude of forward elastic scattering. To such a simple process, axiomatic approaches are possible exploiting the general principles of scattering theory, such as unitarity, analyticity, and crossing symmetry. Therefore a number of theorems and bounds can be derived, which constrain the asymptotic behaviour of the total cross-section in the limit $s \to \infty$. Well-known examples (see Section 4.1) are the Froissart bound, which limits the asymptotic energy dependence of σ_{tot} to a $\ln^2 s$ growth at maximum, and the Pomeranchuk theorem, which states that the ratio of the total cross-sections of particle and antiparticle should tend to unity. Experimental measurements of σ_{tot} at the highest available energies therefore play a fundamental role in probing the setting in of an eventual asymptotic regime.

Total cross-sections cannot be measured at colliding-beam machines by traditional transmission techniques. Three different methods have been used instead, by measuring simultaneously two of the three following quantities: total interaction rate, forward elastic rate, machine luminosity. The most direct method (2) determines σ_{tot} by the ratio between the total interaction rate, measured in a detector with full solid-angle coverage, and the luminosity. A second method (1) exploits the optical theorem, extrapolating to $t = 0$ the measured rate of small-angle elastic scattering. In both cases an absolute calibration of the machine luminosity is required, usually performed either by the van der Meer method (29, 30) or by direct measurements of beam profiles

(31, 32), or even by the measurement of a known electromagnetic process such as Coulomb scattering (33). When a high-precision luminosity calibration is not available, the simultaneous measurement of low-t elastic scattering and of the total rate allows the determination of σ_{tot} without the need for an independent luminosity measurement (34-36). The use of the optical theorem in the second and third methods implicitly assumes that spin effects at small t can be disregarded. The plausibility of this assumption was firmly supported by the precise measurements performed at the ISR, where all three methods were exploited simultaneously (34), obtaining consistent results to an accuracy of better than 1% [see a discussion in Reference (25b)].

Until the coming into operation of the ISR, total cross-sections were believed to approach a finite limit with increasing energy. Actually some hints of a growth were present in cosmic-ray data at very high energy (37) in addition to the well-known rising trend of $\sigma_{tot}(K^+p)$ that was considered as a transient feature. Moreover, the possibility of indefinitely rising hadron cross-sections had also been considered theoretically (38, 39). Nonetheless, the generally-accepted prejudice was that total cross-sections should tend to constant values, and the discovery of the pp rising cross-section at the ISR (1, 2) undeniably came as a surprise. Afterwards, this trend was found to be a general feature of all hadronic total cross-sections. As discussed in Section 2.1.1, the value of ϱ is sensitive to the variation of σ_{tot} with energy, via dispersion relations. The simultaneous study of ϱ and σ_{tot} therefore provides a better understanding of the energy dependence of σ_{tot} and allows a sensible extrapolation in a domain which extends well beyond the accessible energy range. This kind of analysis, pioneered in Reference (7) on ϱ and σ_{tot} data then available up to ISR energies,

was indeed able to predict that the pp and $\bar{p}p$ total cross-sections should keep rising at least up to $\sqrt{s} \approx 300$ GeV at a rate very close to $\ln^2 s$.

Recently, the $\bar{p}p$ total cross-section has been measured at the SPS Collider (36) at an energy as high as $\sqrt{s} = 546$ GeV. The observed value of 61.9 ± 1.5 mb is $\approx 50\%$ higher than at the ISR and indicates that a σ_{tot} rise at a rate compatible with $\ln^2 s$ persists also in this new energy domain. This Collider measurement is shown in Figure 11 together with a compilation of lower energy pp and $\bar{p}p$ total cross-section data which includes the recent $\bar{p}p$ results from the ISR (9, 40). The dispersion relation fit (7) mentioned above is also shown in Figure 11 for comparison (the simultaneous fit to the real part is the curve shown

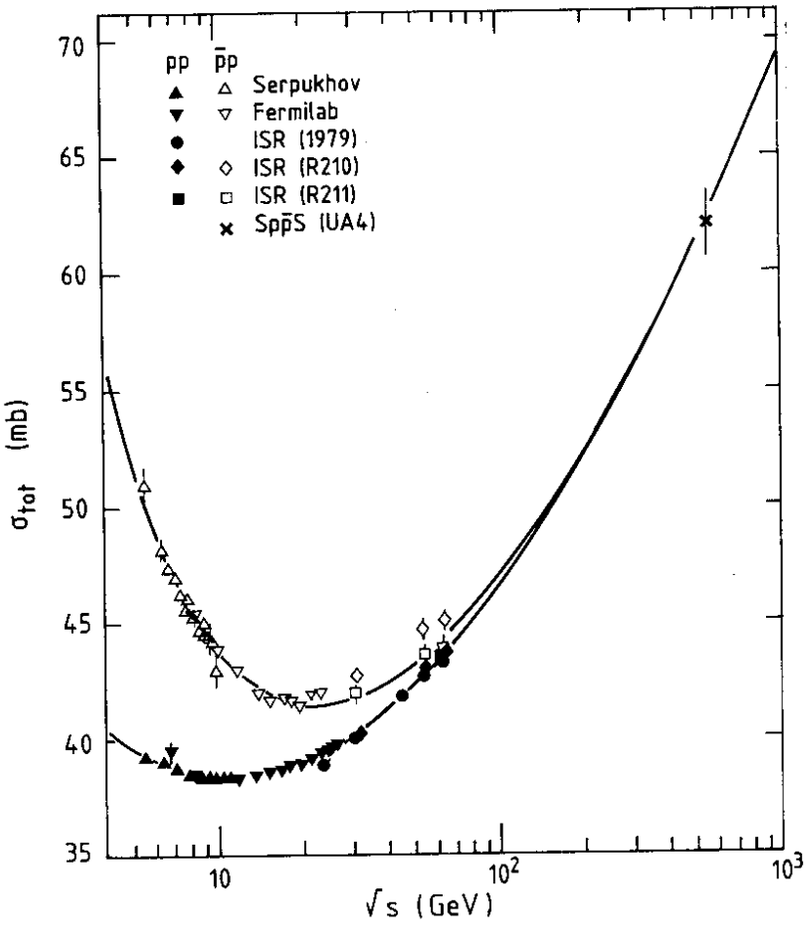

Figure 11. Total cross-section data for pp and $\bar{p}p$ scattering [early, low-statistics measurements at the SPS Collider (18,35) are not shown]. The curve represents the dispersion relation fit of Reference (7).

in Figure 3). One can notice that the recent $\bar{p}p$ data at the highest energies agree well with the prediction of this analysis and their inclusion in fits of this kind confirms the $\ln^2 s$ behaviour of σ_{tot} (4j, 14c). It is striking that data at present energies indicate a rate of growth of σ_{tot} which is just the fastest function allowed at asymptotic energies by the Froissart bound. A suggestive hypothesis is that the observed qualitative saturation of the Froissart bound could be the manifestation of an asymptotic regime, appearing already at present energies, which leads hadron total cross-sections to increase indefinitely at this rate.

At the energy of the Collider the pp and $\bar{p}p$ total cross-sections are expected to have practically the same value. The total cross-section difference $\Delta\sigma = \sigma_{tot}(\bar{p}p) - \sigma_{tot}(pp)$ is shown in Figure 12. Its energy dependence exhibits a Regge behaviour of the kind $s^{-\alpha}$, with $\alpha \approx 1/2$,

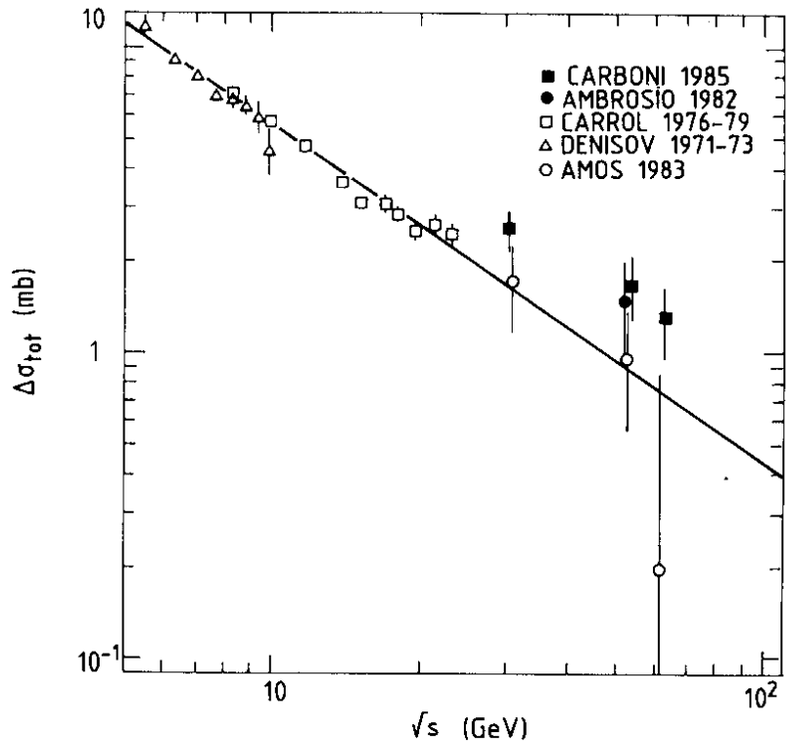

Figure 12. Total cross-section difference $\Delta\sigma = \sigma_{tot}(\bar{p}p) - \sigma_{tot}(pp)$ as a function of energy; the line is a Regge-like fit [from Reference (40b)]

which makes it tend to zero rather rapidly. Actually, if total cross-sections rise indefinitely, their difference does not necessarily have to vanish and might even increase logarithmically with energy, still preserving the limit $\sigma_{tot}(\bar{p}p)/\sigma_{tot}(pp) \to 1$ as required by the Pomeranchuk theorem at infinite energy. Non-vanishing asymptotic contributions (odderons) to the part that is odd under crossing of the forward elastic amplitude, which determines the behaviour of $\Delta\sigma$, have indeed been considered in the literature (41). The operation of the ISR both with proton and antiproton beams has allowed the study of the convergence of pp and $\bar{p}p$ total cross-sections in an energy interval where the difference is expected to become very small. While $\sigma_{tot}(\bar{p}p)$ starts to rise at these energies, the difference $\Delta\sigma$ keeps decreasing following the same inverse power law as observed at lower energy. The ISR data from Reference (40) (black points in Figure 12) could actually suggest a small, systematic deviation above the Regge fit. However, this measurement could include a small but significant electromagnetic inelastic contribution to $\Delta\sigma$ -- up to 0.4 mb according to the authors (40b) -- from which the data of Reference (9) (open circles) are free. As a conclusion, the data are well compatible with the behaviour expected in the framework of a standard Regge exchange picture, with no need for odderons, though a sufficiently small contribution of this kind cannot of course be excluded (see Section 4.1.2).

Data on pp and $\bar{p}p$ total elastic cross-section σ_{el} measured at the ISR and at the SPS Collider, and the corresponding ratio σ_{el}/σ_{tot}, are shown in Figures 13a and 13b, respectively, together with lower energy data. Similarly to σ_{tot}, σ_{el} also starts rising at ISR energies, reaching a value of 13.3 ± 0.6 mb at the SPS $\bar{p}p$ Collider (36). More than

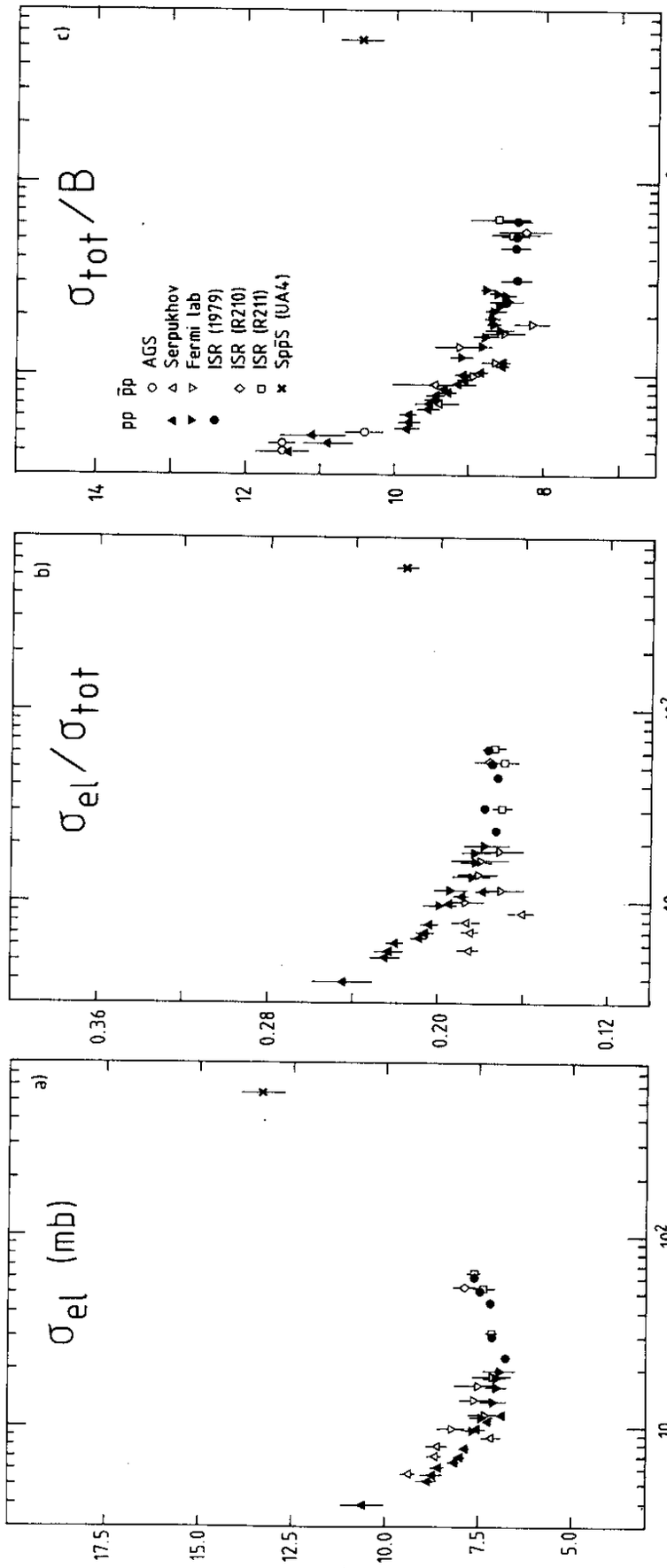

Figure 13. Energy dependence of (a) total elastic cross-section σ_{el}; (b) ratio σ_{el}/σ_{tot}; (c) ratio σ_{tot}/B, for pp and $\bar{p}p$ scattering.

σ_{el} itself, the ratio σ_{el}/σ_{tot} has a crucial role in the investigation of the high-energy regime of hadron scattering, since this parameter is directly sensitive to the hadron opacity. Great interest was aroused a few years ago, when this ratio was found to reach a constant value of about 0.175 over the whole energy range of the ISR (42). This value is below the saturation limit of 0.5, which is typical of a fully absorbing black disc. This was interpreted as the attainment of a 'geometrical scaling' regime in which the proton blackness stabilizes at a rather 'grey' value and the observed $\ln^2 s$ rise of σ_{tot} only reflects a steady expansion of the proton radius like $\ln s$ (see a more detailed discussion in Sections 3.4 and 3.5). However, the validity of this attractive simple picture has been denied by the recent result from the SPS $\bar{p}p$ Collider. The measured value $\sigma_{el}/\sigma_{tot} = 0.215 \pm 0.005$ at $\sqrt{s} = 546$ GeV (36) definitely indicates an increase of the opacity with increasing energy.

A summary of the most relevant parameters of pp and $\bar{p}p$ scattering, at ISR and SPS Collider energies, can be found in Tables 1 to 4. They also include, when available, results on the direct comparison of pp and $\bar{p}p$ data measured by the same experiment, in particular on the following quantities: $\Delta\sigma_{tot} = \sigma_{tot}(\bar{p}p) - \sigma_{tot}(pp)$, $\Delta\varrho = \varrho(\bar{p}p) - \varrho(pp)$ and $\Delta B = B(\bar{p}p) - B(pp)$.

It is worth stressing that the energy dependence of the parameter σ_{el}/σ_{tot} is crucial in order to discriminate between the various theoretical models that claim to describe the asymptotic behaviour of hadron scattering. These can be classified coarsely in three groups (43): in addition to the 'geometrical scaling' approach mentioned above, in which the ratio σ_{el}/σ_{tot} is expected to be energy independent, other models have been developed in which this parameter is predicted either to decrease or to increase with energy. In the Reggeon Field Theory with

Table 1 pp scattering

$\sqrt{s}$ (GeV)	σ_{tot} (mb)	σ_{el} (mb)	σ_{el}/σ_{tot}	σ_{tot}/B
23	38.94 ± 0.17	6.73 ± 0.08	0.1728 ± 0.0016	8.47 ± 0.15
31	40.14 ± 0.17	7.16 ± 0.09	0.1784 ± 0.0017	8.45 ± 0.14
45	41.79 ± 0.16	7.17 ± 0.09	0.1716 ± 0.0018	8.38 ± 0.13
53	42.67 ± 0.19	7.45 ± 0.09	0.1746 ± 0.0016	8.37 ± 0.13
62	43.32 ± 0.23	7.66 ± 0.11	0.1768 ± 0.0021	8.36 ± 0.13
Ref.	(42)[a]	(42)[b]	(42)	(34, 42)

a Scale error ± 0.25 mb
b Scale error ± 0.09 mb

Table 2 pp elastic scattering

$\sqrt{s}$ (GeV)	ϱ	B (GeV^{-2})	B'(-t > 0.15) (GeV^{-2})
23	0.02 ± 0.05	11.8 ± 0.2	10.3 ± 0.2
31	0.042 ± 0.011	12.2 ± 0.2	10.9 ± 0.2
45	0.062 ± 0.011	12.8 ± 0.2	11.0 ± 0.2
53	0.078 ± 0.010	13.1 ± 0.2	10.7 ± 0.2
62	0.095 ± 0.011	13.3 ± 0.2	10.4 ± 0.2
Ref.	(42)[a]	(34)	(34)

a Scale error ± 0.015

Table 3 $\bar{p}p$ scattering

$\sqrt{s}$ (GeV)	σ_{tot} (mb)	σ_{el} (mb)	σ_{el}/σ_{tot}	σ_{tot}/B	$\Delta\sigma_{tot}$ (mb)	Ref.
31	42.0 ± 0.5	7.14 ± 0.17	0.170 ± 0.005	--	1.7 ± 0.5	(9)
31	42.8 ± 0.35	--	--	--	2.58 ± 0.41	(40)
53	43.65 ± 0.41	7.36 ± 0.30	0.169 ± 0.007	8.39 ± 0.34	0.98 ± 0.36	(9)
53	44.71 ± 0.46	7.89 ± 0.28	0.176 ± 0.007	8.25 ± 0.36	1.70 ± 0.53	(40)
62	43.9 ± 0.6	7.62 ± 0.19	0.174 ± 0.005	8.61 ± 0.41	0.2 ± 0.6	(9)
62	45.14 ± 0.38	--	--	--	1.32 ± 0.48	(40)
546	61.9 ± 1.5	13.3 ± 0.6	0.215 ± 0.005	10.5 ± 0.3	--	(36)

Table 4 $\bar{p}p$ elastic scattering

$\sqrt{s}$ (GeV)	ϱ	B (GeV^{-2})	B'(-t > 0.15) (GeV^{-2})	$\Delta\varrho$	ΔB (GeV^{-2})	Ref.
31	0.065 ± 0.025	--	--	0.036 ± 0.027	--	(9)
31	--	--	11.16 ± 0.20	--	--	(13a)
53	0.101 ± 0.018	13.36 ± 0.53	--	0.042 ± 0.020	0.51 ± 0.54	(9)
53	--	13.92 ± 0.59	10.68 ± 0.26	--	0.83 ± 0.83	(40)
53	--	--	11.50 ± 0.15	--	--	(13a)
62	0.12 ± 0.03	13.1 ± 0.6	--	0.04 ± 0.03	0.1 ± 0.6	(9)
62	--	--	11.12 ± 0.15	--	--	(13a)
546	--	15.2 ± 0.2	13.4 ± 0.3	--	--	(16)

'critical Pomeron' (44) the opacity, and thus σ_{el}/σ_{tot}, decreases with increasing energy, while the expansion of the radius prevents σ_{tot} from decreasing. This approach seems now to be excluded by the Collider measurements. In the 'factorizing eikonal' models, as discussed in Section 4.3, the asymptotic regime is still far away in energy, although σ_{tot} already increases with a dependence close to $\ln^2 s$: the opacity is also increasing slowly with energy, so that hadrons tend gradually to become completely black discs. The ratio σ_{el}/σ_{tot} is therefore predicted to reach the value 1/2 at infinite energy [the 'supercritical string' model (45) also exhibits similar features]. The recent findings at the SPS $\bar{p}p$ Collider clearly favour the latter class of models.

Another parameter often used to probe the asymptotic behaviour of hadron scattering, which however is not independent of σ_{el}/σ_{tot} (see Section 4.1.4), is the ratio σ_{tot}/B. Similarly to the former, the latter is also sensitive to the hadron opacity. The trend of this quantity is illustrated in Figure 13c up to Collider energy and appears to be similar to that of σ_{el}/σ_{tot}. After reaching a constant plateau in the ISR energy range at about 8.4 it rises again up to $\sigma_{tot}/B = 10.5 \pm 0.3$ at $\sqrt{s} = 546$ GeV.

As a conclusion, the measurements at the nowadays highest available energies consistently indicate that the hadron opacity, which was believed to have definitely reached a constant value already at ISR energies, is actually increasing: hadrons become not only larger, but also darker as energy increases. Despite the observed qualitative saturation of the Froissart bound, there is still a long way to go in the approach to the elusive asymptopia.

3. INTERPRETATION OF HADRON SCATTERING AT HIGH ENERGY

3.1 Notations and Kinematics of Scattering Processes

In the S-matrix formalism, the most general operator which leads from the initial state $|i\rangle$ to a final state $|f\rangle$ can be written as

$$\langle f|1 + iT|i\rangle = \delta_{fi} + i(2\pi)^4 \delta^4(P_f - P_i) \frac{\langle f|F|i\rangle}{\sqrt{\Pi_n^{(f)}(2E_n)\ \Pi_m^{(i)}(2E_m)}} \,. \qquad 2.$$

In Equation 2 the running products Π_j of the initial and final energies (E_m, E_n, respectively) separate the Lorentz-invariant part F of the transition matrix T, and the energy and momentum conservation is explicitly required by the δ-function of the initial and final total four-momenta P_i and P_f (spins are disregarded, as discussed previously). The cross-section for a process where two particles with masses m_1, m_2 give rise to a final state with an arbitrary number of particles ($1 + 2 \rightarrow 3 + 4 + \ldots + N$) takes the following form:

$$\sigma_{fi} = \frac{1}{4\sqrt{(p_1 \cdot p_2)^2 - (m_1 m_2)^2}} \int (2\pi)^4 \delta^4(P_f - P_i) |F_{fi}|^2 \prod_{n=3,N} \frac{d^3\vec{p}_n}{(2\pi)^3\ 2E_n} \,, \qquad 3.$$

where p_j is the four-momentum of the j-th particle.

When one considers the particular case of a two-body reaction ($1 + 2 \rightarrow 3 + 4$), Equation 3 becomes

$$\sigma_{fi} = (1/k_i) \int (1/8\pi W)^2 |F_{fi}|^2 k_f \, d\Omega_{cm} \,. \qquad 4.$$

Here k_i and k_f are the c.m. momenta of the particles in the initial and in the final state, respectively, and W is the total c.m. energy. For elastic scattering, one has $k_f = k_i = k$ and therefore the differential cross-section per unit solid angle $d\Omega_{cm}$ around the scattering angle θ can be expressed as

$$d\sigma/d\Omega_{cm} = (1/8\pi W)^2 |F(W,\theta)|^2 \quad . \qquad 5.$$

It is convenient to write all physical quantities in terms of the Lorentz-invariant Mandelstam variables s, t, u:

$$s = (p_1 + p_2)^2 = W^2$$

$$t = (p_1 - p_3)^2 = -2k^2(1 - \cos\theta)$$

$$u = (p_1 - p_4)^2 = -2k^2(1 + \cos\theta) + (m_1^2 - m_2^2)^2/W^2 =$$

$$= m_1^2 + m_2^2 + m_3^2 + m_4^2 - s - t \quad .$$

Since we are interested in the asymptotic behaviour at high energies, from now on we shall assume $k^2 \gg m_i^2$ and thus $s \simeq 4k^2$ and $dt \simeq (s/4\pi)\, d\Omega_{cm}$. In this limit, Equation 5 reads

$$d\sigma/dt = (1/16\pi s^2)|F(s,t)|^2 \quad . \qquad 6.$$

3.2 Unitarity and the Optical Theorem

Probability conservation implies the unitarity of the S matrix: $S^+S = SS^+ = 1$. Since $S = 1 + iT$, one has $i(T^+ - T) = TT^+$, and therefore

$$2\ \mathrm{Im}\ \langle f|T|i\rangle = \Sigma_l \langle f|T|l\rangle\langle l|T^+|i\rangle =$$

$$= \Sigma_m^{(inel)} \langle f|T|m\rangle\langle m|T^+|i\rangle + \Sigma_n^{(el)} \langle f|T|n\rangle\langle n|T^+|i\rangle \quad , \qquad 7.$$

where the sum over all possible intermediate states $|l\rangle$ has been split into separate sums over the inelastic and the elastic channels. Equation 7 acquires a special meaning when the initial and final states are the same ($|i\rangle \equiv |f\rangle$, as for elastic scattering at $\theta = 0$):

$$2\ \mathrm{Im}\ F_{ii} = \sum_m^{(inel)} \int (2\pi)^4 \delta^4(P_i - P_m) |F_{im}|^2 \prod_j \frac{d^3\vec{p}_j}{(2\pi)^3\, 2E_j} +$$

$$+ \frac{4W^2k^2}{E_1E_2} \int \frac{|F_{in}(\theta)|^2}{(8\pi W)^2}\, d\Omega \quad . \qquad 8.$$

The two terms in Equation 8 can be recognized as the quantities defined in Equations 3 and 5, i.e. the inelastic and elastic cross-sections respectively. Equation 8 is therefore the well-known optical theorem, which is more simply written as

$$\text{Im } F(\theta = 0) = 2Wk(\sigma_{inel} + \sigma_{el}) \simeq s\sigma_{tot} \ . \qquad 9.$$

In general, as a consequence of unitarity, for elastic scattering at $t \neq 0$ (i.e. $|i\rangle \neq |f\rangle$) one can write

$$\text{Im } F(t) = s[G_{inel}(t) + G_{el}(t)] \ , \qquad 10.$$

where $G_{inel}(t)$ and $G_{el}(t)$ are the inelastic and elastic overlap functions (46) introduced by Van Hove. These functions are so normalized that $G_{inel}(0) = \sigma_{inel}$ and $G_{el}(0) = \sigma_{el}$.

3.3 Impact Parameter Representation

Let us consider the standard partial-wave expansion of the scattering amplitude F:

$$F(s, \cos\theta) = (8\pi W/k) \sum_l (2l + 1) f_l(s) P_l(\cos\theta) \ , \qquad 11.$$

where $f_l(s)$ is the l-th partial wave amplitude and $P_l(\cos\theta)$ is the Legendre polynomial of order l. Since at very high energy a great number of partial waves contribute to F, it is legitimate to replace the sum over l by an integral over the bidimensional impact parameter $\vec{b}$ [with $|\vec{b}| = (l + 1/2)/k$]. Equation 11 thus becomes

$$\frac{F(s,q^2)}{8\pi s} = \frac{1}{2\pi} \int f(b) \, e^{i\vec{q}\cdot\vec{b}} \, d^2\vec{b} = \int f(b) \, J_0(qb) \, b \, db \ , \qquad 12.$$

where $q = k_1 - k_3$ is the momentum transfer ($q^2 = -t$). The amplitude f(b) can then be obtained from the inversion of Equation 12, by the known properties of Fourier transforms:

$$f(b) = \frac{1}{2\pi} \int \frac{F(s,q^2)}{8\pi s} e^{-i\vec{q}\cdot\vec{b}} d^2\vec{q} = \int \frac{F(s,q^2)}{8\pi s} J_0(qb)\, q\, dq \ . \qquad 13.$$

The unitarity condition 10 in the impact parameter space then reads:

$$\text{Im } f(s,b) = |f(s,b)|^2 + \frac{1}{4} G_{inel}(s,b) \ . \qquad 14.$$

Im f(s,b) is usually referred to as the profile function, and represents the hadronic opacity as a function of the impact parameter b. The meaning of unitarity relation 14 is particularly simple when integrated over b, and reduces to $\sigma_{tot} = \sigma_{el} + \sigma_{inel}$, since from Equations 9 and 12 one has:

$$\sigma_{tot} = 8\pi \int \text{Im } f(s,b)\, b\, db \ , \qquad 15.$$

$$\sigma_{el} = 8\pi \int |f(s,b)|^2\, b\, db \ , \qquad 16.$$

$$\sigma_{inel} = 8\pi \int 1/4\, G_{inel}(s,b)\, b\, db \ . \qquad 17.$$

In its differential form (Equation 14), unitarity relates the elastic and inelastic cross-sections at the same value of b: $d^2\sigma_{tot}/db^2 = d^2\sigma_{el}/db^2 + d^2\sigma_{inel}/db^2$. This is often referred to by saying that 'unitarity is diagonal in impact parameter space'. Equation 14 puts a limit on the inelastic overlap function: $G_{inel} \leq 1$. In addition, since G_{inel} is positive, the unitarity condition 14 implies:

$$0 \leq |f(s,b)|^2 \leq \text{Im } f(s,b) \leq 1 \ . \qquad 18.$$

A relevant physical consequence of Equation 14 is that no scattering process can be uniquely inelastic: a non-vanishing elastic scattering amplitude must always be present as a 'shadow' of all the inelastic channels open at that energy. The forward elastic peak can thus be seen as analogous to the diffraction pattern arising in classical optics when a plane wave encounters an absorbing disc. As energy increases, elastic scattering is indeed expected to become purely diffractive, as small as allowed by Equation 14 for a given G_{inel}. The elastic amplitude then tends to be purely imaginary, and the smaller of the two solutions of Equation 14 is assumed to correspond to the physical situation. In this case the upper bound 18 is lowered to Im $f(s,b) \leq 1/2$.

In order to satisfy the unitarity relation 14 it is convenient to express the amplitude $f(s,b)$ in terms of the complex eikonal function $\chi(s,b)$:

$$f(s,b) = i(1 - \exp [i\chi(s,b)])/2 \ , \qquad 19.$$

where Im $\chi \geq 0$ and the inelastic overlap function is recognized to be $G_{inel} = 1 - \exp(-2 \text{ Im } \chi)$. For Im $\chi = 0$, G_{inel} vanishes: this is the case when the reaction is below the threshold of all inelastic channels. At high energy we are rather dealing with the opposite case: elastic scattering is essentially diffractive, and Re χ is small. If Re $\chi = 0$, the amplitude f is purely imaginary and determined by the opaqueness $\Omega(s,b) = \text{Im } \chi$. In the limit $\Omega \to \infty$ the inelastic absorption is maximum and Im f approaches the reduced unitarity bound of 1/2. This is the case for a completely black disc; the elastic cross-section is then also maximum and reaches the value (see Equations 15 to 17):

$$\sigma_{el} = \sigma_{inel} = \frac{1}{2} \sigma_{tot} \ . \qquad 20.$$

3.4 Overlap Function Analysis of pp Scattering at the ISR

The geometrical representation outlined in the previous Section provides an easy, intuitive framework which is independent of the underlying dynamics. Hadron elastic differential cross-sections do exhibit diffraction patterns quite similar to those observed in optics. As shown in Figure 14c, this phenomenon becomes surprisingly evident when the scatterer is a complex nucleus, which has rather well defined dimensions. The profile

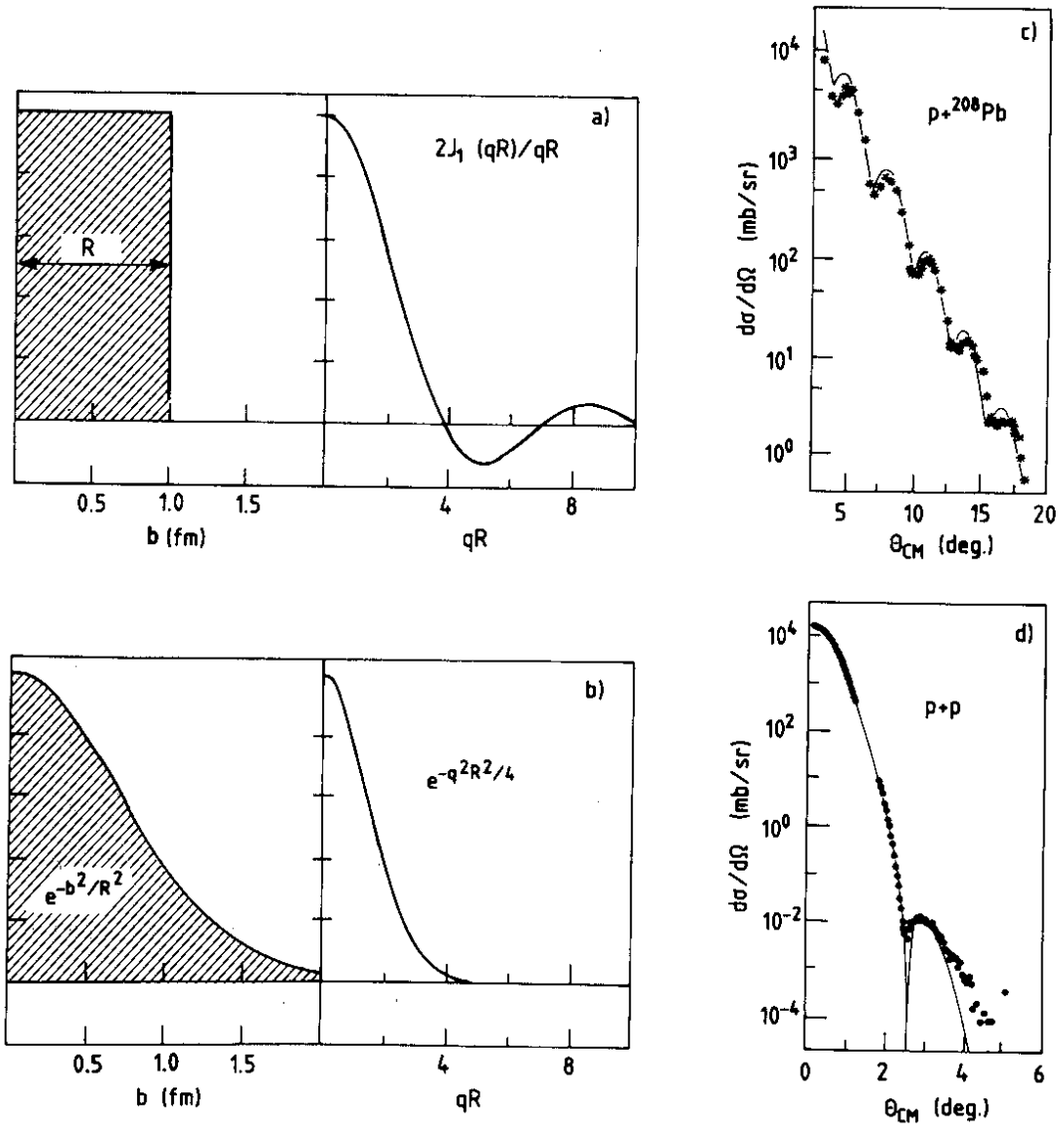

Figure 14. (a),(b) Examples of profile functions and corresponding scattering amplitudes; (c),(d) diffraction patterns observed in hadron scattering [from Reference (4g)].

function f(b) of a heavy nucleus closely resembles that of a uniformly opaque disc, whose Fourier transform (Equation 12) is a Bessel function $J_1(qR)$, R being the disc radius. Such an amplitude indeed shows a series of zeros with the increase of the momentum transfer q, as illustrated in Figure 14a.

A qualitatively different picture is observed when the scatterer is a single proton. In this case the elastic differential cross-section exhibits a monotonous, exponential decrease in t, down to $|t| \approx 1.4\ GeV^2$, over about six orders of magnitude (see Figure 14d). This apparently inconsistent behaviour is however easily reconciled when one considers that an exponential in t is precisely the Fourier transform of a Gaussian profile function, as shown in Figure 14b. From this point of view, the difference between a massive nucleus and a single proton lies just in the different sharpness of the edges! In a simplified calculation, if one neglects the real part of the elastic scattering amplitude and moreover assumes that the differential cross-section can be parametrized by a single exponential with slope B, by the optical theorem (Equation 9) one can write the elastic amplitude in the form $F(s,t) = is\sigma_{tot} \exp(-B|t|/2)$. The profile function, derived by Equation 13, is then:

$$f(b) = (i/8\pi)\ (\sigma_{tot}/B)\ \exp(-b^2/2B)\ . \qquad 21.$$

Let us go further, and consider a quantitative analysis of pp elastic scattering data, already shown in Figure 1. In order to compute the profile function Im f(s,b) from Equation 13,

$$\text{Im } f(s,b) = (1/4\sqrt{\pi}) \int dt\ J_0(b\sqrt{-t})\ \{d\sigma/dt - (1/16\pi s^2)[\text{Re } F(s,t)]^2\}^{1/2}\ , \qquad 22.$$

an estimate of the real part of the elastic scattering amplitude at $t \neq 0$ is needed. It should, however, be noticed that the real part has little effect, because at any given value of b the integral in Equation 22 is dominated by the contribution at low t, where the real part is known to be small. Therefore the determination of the profile function does not depend critically on any sensible choice. A reasonable parametrization of the real part of the elastic scattering amplitude at ISR energies [see for instance Reference (42)] takes into account the measured values of ϱ, vanishes at $t \approx 0.2$ GeV^2 to satisfy dispersion relation analysis (47) and correctly fills the dip at $t \approx 1.4$ GeV^2, where the imaginary part is supposed to be vanishing. At all values of t, anyhow, the real part turns out to be much smaller than the imaginary part, except of course in the dip region. With a reasonable assumption for the real part, by Equation 22 the profile function Im f(s,b) can be computed numerically from the $d\sigma/dt$ data: the inelastic overlap function G_{inel} (s,b) is then obtained by Equation 14.

The results of such an analysis (48-52) performed on the data at $\sqrt{s} = 53$ GeV are displayed in Figure 15. The profile function exhibits a shape which is very close to a Gaussian in b, as expected from the approximately exponential behaviour of $d\sigma/dt$. Its r.m.s. width, corresponding to the effective proton radius, is found to be slightly less than 1 fm at this energy. One can notice that Im f(b) has a maximum value of 0.36, which is far from the unitarity limit of 0.5: this means that even in a central collision at $b = 0$ a target proton is not completely dark, but the projectile has a non-vanishing probability of going straight through without interacting. The presence of the dip structure in $d\sigma/dt$ at $t \approx 1.4$ GeV^2 produces a slight flattening of the profile function with respect to a Gaussian (too small to be visible in the

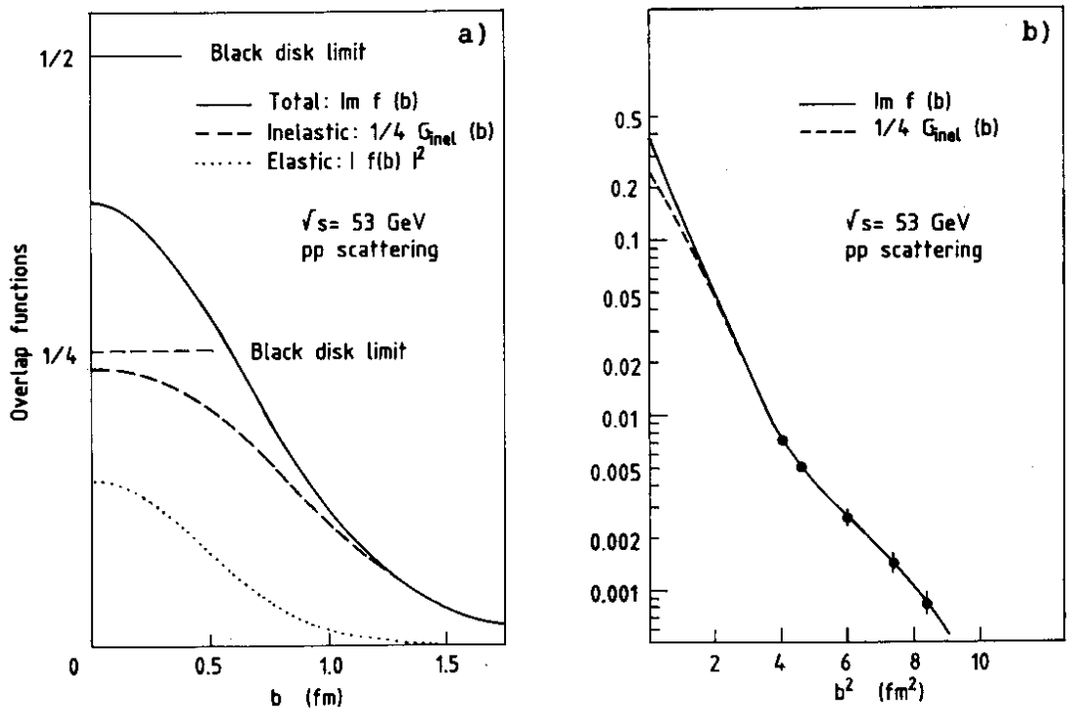

Figure 15. Total, inelastic and elastic overlap functions of pp scattering at $\sqrt{s}$ = 53 GeV (50, 52). The deviation of the tail from a Gaussian is evidenced by the logarithmic scale.

figure) at very small values of b. One should realize that a sharp black disc with a radius of 1 fm would produce a first dip in $d\sigma/dt$ at $t \approx 0.6$ GeV^2 (see Figure 14a). In the interval from this value of t to the measured position of the dip, the elastic amplitude decreases by two other orders of magnitude. It should then not be surprising that the striking structure in $d\sigma/dt$ can hardly be noticed in the profile function: the dip at 1.4 GeV^2 is simply too far to modify significantly the basic Gaussian shape of Im f(b). On the contrary, the slight variation of the slope of $d\sigma/dt$ at $-t \approx 0.13$ GeV^2, though less striking, brings a distortion to the tail of Im f(b) above 2 fm that is almost one order of magnitude higher than the Gaussian (see Figure 15b).

The same qualitative features are exhibited by the inelastic overlap function $G_{inel}(b)$, which is related to the profile function by the unitarity relation 14. According to this equation, the tails of

1/4 G_{inel} and of Im f are essentially identical at large values of b, where the term $|f|^2$ is negligible, while near b = 0 the inelastic overlap function flattens with respect to the profile function.

Detailed analyses of the energy dependence of G_{inel} over the ISR range have been performed (42, 53). In particular, a systematic study based on a critical review of available ISR data has been carried out by the authors of Reference (42). They have selected elastic $d\sigma/dt$ data from several ISR experiments, readjusted the absolute normalizations taking into account the general trend of the differential cross-section, and interpolated between neighbouring data sets in those t-ranges in which no measurement was available. The experimental data they used at the five ISR energies have been shown in Figure 1. Their results indicate that the observed $\ln^2 s$ rise of σ_{tot} over the ISR energy range only comes from an increase of the interaction radius which is linear in ln s, while the central opacity remains practically constant. As a matter of fact, the variation $\Delta G_{inel}(b)$, which from zero at b = 0 reaches a maximum around b ≈ 1 fm (see Figure 16a), essentially

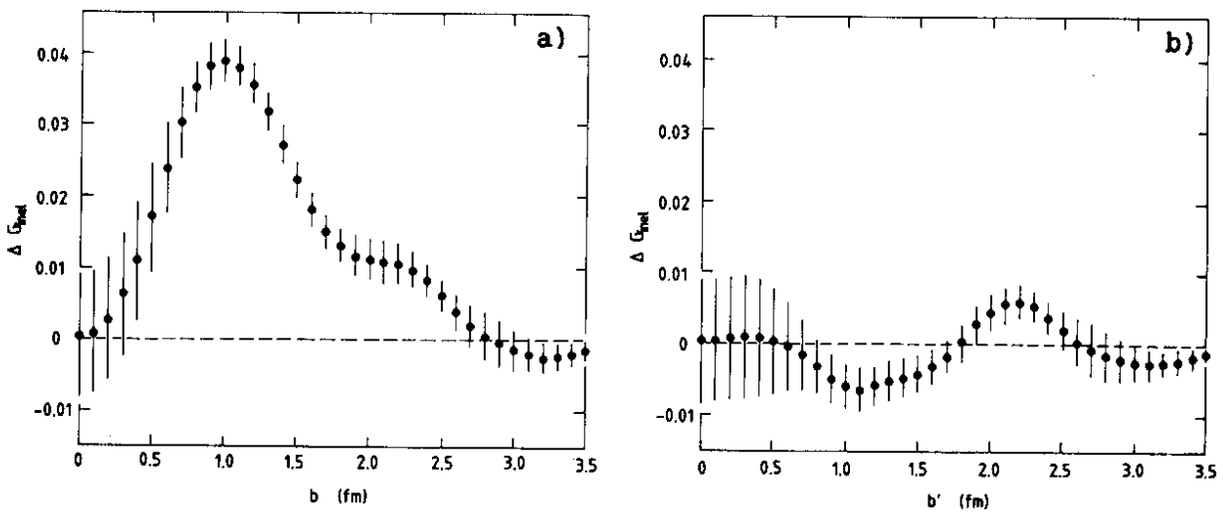

Figure 16. Variation ΔG_{inel} of the pp inelastic overlap function over the ISR energy range (a) as a function of the impact parameter b; (b) as a function of the reduced impact parameter $b' = b/[\sigma_{tot}(s)/38.94\ mb]^{1/2}$ [from Reference (42)].

disappears when the impact parameter is rescaled according to the mean interaction radius or, equivalently, to the square root of the total cross-section. Indeed, if G_{inel} is expressed in terms of the reduced impact parameter $b' = b/\sqrt{\sigma_{tot}}$, one obtains an energy independent pattern. This is illustrated in Figure 16b, where the energy variation $\Delta G_{inel}(b')$ of the inelastic overlap function over the ISR energy range, as a function of the reduced impact parameter, appears to be consistent with zero.

3.5 The Geometrical Scaling Hypothesis confronted with SPS Collider Data

As discussed in the previous section, the ISR pp elastic scattering data suggest that, as energy increases, the central blackness remains constant, while the edge of the overlap function moves towards larger values of b. It is therefore natural to consider a simple model in which the only effect produced on the profile function f(s,b) by varying the energy is a change in the mean interaction radius R. This so-called 'geometrical scaling' hypothesis can be expressed as follows:

$$f(s,b) = f'(b/R) \ . \qquad 23.$$

After defining the reduced impact parameter $b' = b/R$, Equation 12 becomes

$$F(s,t)/8\pi s = R^2 \int_0^\infty f'(b')J_0(Rb'\sqrt{-t})\ b'\ db' = R^2F'(R^2t) \ , \qquad 24.$$

where F' does not depend any more separately on s and t, but only on the adimensional variable tR^2, with R depending on energy. A direct consequence of Equation 24, via the optical theorem (Equation 9), is that the energy dependence of the total cross-section only comes from the

variation of R with energy: $\sigma_{tot}(s) \propto R^2(s)$. If $\tau = t\sigma_{tot}$ is chosen as the scaling variable, it follows from Equation 24 that the quantity (see Equation 6)

$$(1/\sigma_{tot})\, d\sigma_{el}/d\tau = \varphi(\tau) \qquad 25.$$

has a universal shape independent of energy. As a consequence, the local slope parameter $B = (d/dt) \ln (d\sigma/dt)$ can be written as $\sigma_{tot}(d/d\tau) \ln [\varphi(\tau)]$ and, therefore,

$$\sigma_{tot}/B = \text{const.} \qquad 26.$$

In particular, it also follows that the position of the dip and the height of the secondary maximum respectively go like

$$|t_{dip}| \sim 1/\sigma_{tot} \quad \text{and} \quad d\sigma/dt|_{t=t_2} \sim \sigma_{tot}^2 .$$

In addition

$$\sigma_{el}/\sigma_{tot} = \int \varphi(\tau)\, d\tau = \text{const.} \qquad 27.$$

Indeed elastic-scattering data at the ISR seem to support this hypothesis. Figure 8b shows how elastic differential cross-sections $(1/\sigma_{tot})\, d\sigma/d\tau$ measured at the two extreme ISR energies fall one on top of the other. Also the ratio σ_{el}/σ_{tot}, shown in Figure 13b, although decreasing at lower energies, seems to become constant in the ISR energy range. The same tendency of approaching a constant value is observed in the behaviour of the ratio σ_{tot}/B up to ISR energies (see Figure 13c).

This nice picture unfortunately fails when the energy span is extended far beyond the ISR range. As a matter of fact, the recent measurement of the ratio σ_{el}/σ_{tot} at the $\bar{p}p$ Collider is definitely larger than at

the ISR and incompatible with the assumption of constancy (expressed by Equation 27) as discussed in Section 2.2 and shown in Figure 13b. The increase of this parameter directly indicates that the opacity of $\bar{p}p$ interaction is actually rising, after the seeming plateau observed in the ISR energy range. The same conclusion is, of course, drawn from the behaviour of the parameter σ_{tot}/B, which is also proportional to the nucleon opacity (see the simplified example of Equation 21) and is found to increase sensibly in the same energy interval, as can be seen in Figure 13c. This violation of geometrical scaling appears quite evident in a detailed analysis of the overlap function $G_{inel}(b)$ (54). Here, in addition to a clear expansion of the interaction radius, the central opacity is also found to be definitely larger than at ISR energies, closely approaching the unitarity limit of one. Even rescaled in the reduced impact parameter b' [as was done for the ISR data in the analysis (42) quoted in the previous section], $G_{inel}(b')$ exhibits a clear energy dependence when going from the ISR to the SPS Collider. This behaviour is clearly shown in Figure 17, in which the energy variation

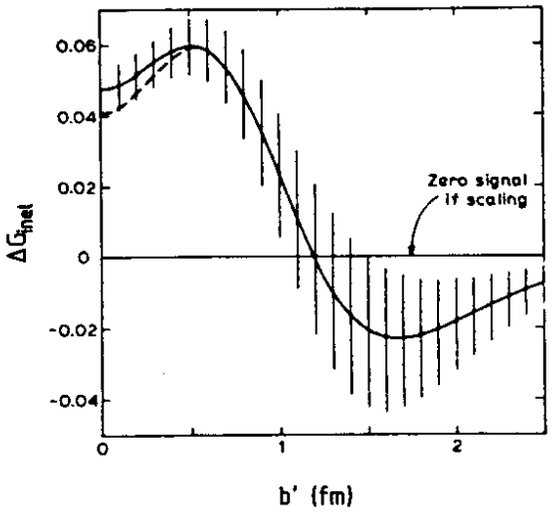

Figure 17. Variation ΔG_{inel} of the inelastic overlap function from ISR to SPS Collider energy, as a fuction of the reduced impact parameter $b' = b/[\sigma_{tot}(s)/61.9\ mb]^{1/2}$ [from Reference (54)].

$\Delta G_{inel}(b')$ from $\sqrt{s}$ = 53 GeV to $\sqrt{s}$ = 546 GeV is found to be incompatible with a zero level. This picture has to be compared with Figure 16b where the same quantity, evaluated over the ISR energy span, appears to be consistent with zero. One can conclude that there is clear evidence that the nucleon, which at the ISR just seemed to become larger, is also getting blacker as energy increases. The observed rise of σ_{tot} is therefore not only due to the expansion of the interaction radius but also to an increase of the nucleon darkness.

4. THE VERY HIGH ENERGY LIMIT

It is reasonable to assume that at sufficiently high energy the features of hadron scattering can be interpreted in a simple way in terms of a few general theoretical principles, independently of specific models. Asymptotic properties of the scattering amplitudes can indeed be derived from the requirements of unitarity, analyticity, and crossing symmetry. This kind of approach, pioneered by Pomeranchuk (55) and by Froissart (56) has led to several theorems which impose non-trivial constraints on hadron behaviour at asymptotic energies [the interested reader can find a complete review in References (4d) and (4i)].

4.1 Asymptotic Theorems

4.1.1. FROISSART-MARTIN BOUND The well-known Froissart-Martin upper bound (56) on total cross-section has been derived from axiomatic field theory (57, 58a) and states that

$$\sigma_{tot} \leq (\pi/m_\pi^2) \ln^2 s \ . \qquad 28.$$

An intuitive idea of the physical meaning of this theorem can be obtained in impact parameter representation. In order to satisfy analyticity, the

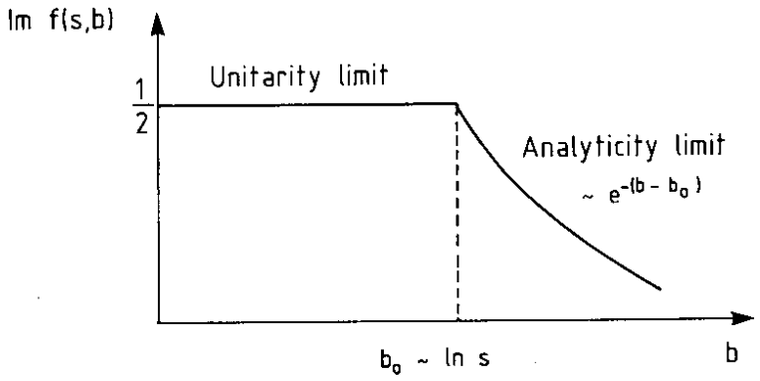

Figure 18. Upper bound to the profile function.

profile function has been shown to be limited by an exponential decrease with increasing values of the impact parameter, and by a rather slow increase with energy, of the kind Im $f(s,b) \leq$ const s^{β} exp $(-2m_{\pi}b)$ with $\beta \leq 1$. In the case of diffraction scattering, however, the reduced unitarity limit Im $f(s,b) \leq 1/2$ cannot be exceeded (see Section 3.3). The upper bound shown in Figure 18 is thus obtained:

$$\text{Im } f(s,b) = 1/2 \qquad \text{for } b \leq b_0$$

$$\text{Im } f(s,b) = \exp\left[-2m_{\pi}(b - b_0)\right] \qquad \text{for } b > b_0 \ ,$$

where $b_0 = (1/2m_{\pi}) \ln (s/s_0)$. Using Equation 15 one then obtains the upper limit 28, which corresponds to a full absorption of all partial waves up to b_0: the surface of this black disc increases as $\ln^2 s$. The grey fringe for $b > b_0$ imposed by analyticity has a constant width, so that its surface increases only as ln s and has a negligible role in the upper bound 28 at infinite energy.

It is worth noticing that Equation 28 is indeed a minimum upper bound which by no means can be further restricted. For some time, before rising cross-sections were discovered at the ISR, when people believed that hadrons had an asymptotically constant size, theoreticians tried

to lower the bound and to prove that total cross-sections were asymptotically limited by a constant. This effort was revealed to be hopeless when an example was found by constructing a crossing symmetric amplitude (59) which satisfies unitarity and analyticity, and behaves like $s \ln^2 s$ in the forward direction.

ISR and Collider σ_{tot} data are indeed compatible with a $\ln^2 s$ rise (see Figure 11), although with a coefficient much smaller than in Equation 28. This behaviour may lead to the belief that an asymptotic regime is already installed at presently available energies and that the Froissart bound is indeed qualitatively saturated by nature, if not quantitatively. This might suggest that, for some reason, the profile function of the nucleon is bound not to exceed the 'greyness' we observe today and the rise of the total cross-section simply reflects the expansion of the proton radius. This hypothesis was indeed supported by the geometrical scaling behaviour found in the ISR data, as discussed in Section 3.4. The recent measurement at the SPS Collider indicates, on the contrary, that the ratio σ_{el}/σ_{tot} does not remain constant beyond ISR energies and that the hadronic opacity is actually slowly increasing with s. One has, however, to remember that in the limit of a completely saturated black disc the ratio σ_{el}/σ_{tot} must approach 1/2, which also at the Collider is far from being the case: even at b = 0 the profile function is still sensibly lower than the reduced diffractive limit of 1/2 imposed by unitarity. Therefore, if the nucleon becomes blacker and blacker as energy increases, since it is still far from the quantitative saturation of the Froissart bound, there might be a very long way to an asymptotic regime and the present $\sim \ln^2 s$ behaviour could just be a transient accident with no deep meaning.

4.1.2 POMERANCHUK THEOREM On a phenomenological basis, one observes that the total cross-section $\sigma_{tot}(ab)$ of hadron 'a' hitting target 'b' and the total cross-section $\sigma_{tot}(\bar{a}b)$ of the corresponding antiparticle hitting the same target, approach each other more and more as energy increases (see, for instance, Figures 11 and 12). In its original formulation, based on dispersion relations for the forward-scattering amplitude, the Pomeranchuk theorem (55) stated that if the total cross-sections of particle and antiparticle tend to a constant with increasing energy, their difference tends to zero. At the time in which the total cross-sections were indeed believed to approach a constant limit, everybody was happy with this formulation of the theorem, which seemed to be confirmed by experiment. However, this formulation is of no use if the rising total cross-sections discovered at the ISR are interpreted as the onset of an asymptotic behaviour of everlasting growth. Therefore many authors (60) have worked at a reformulation of the theorem in order to preserve the final statement, which still appeared to be supported by experimental evidence, by trying to exploit analyticity and unitarity without adopting additional restrictive assumptions. This method finally led to proving that if at least one cross-section rises indefinitely [either $\sigma_{tot}(\bar{a}b) \to \infty$ or $\sigma_{tot}(ab) \to \infty$], then

$$\sigma_{tot}(\bar{a}b)/\sigma_{tot}(ab) \to 1 \qquad 29.$$

for $s \to \infty$. It should be noted that this formulation does not imply that the total cross-section difference $\Delta\sigma = \sigma_{tot}(\bar{a}b) - \sigma_{tot}(ab)$ goes to zero. Equation 29 in fact cannot even exclude that $\Delta\sigma$ goes to infinity as energy increases. Some authors have indeed considered the possibility that the imaginary part of the odd-signature amplitude $F^- = F^{\bar{a}b} - F^{ab}$

at t = 0, to which $\Delta\sigma$ is proportional, grows as fast as ln s (41). The recent data on $\sigma_{tot}(pp)$ and $\sigma_{tot}(\bar{p}p)$ from the ISR, however, disfavour this hypothesis (see Figure 12). Another possibility is that the asymptotic odd-signature contribution to $\Delta\sigma$ remains constant with increasing energy [see a discussion in Reference (61)]. An even more subtle hypothesis assumes that the amplitude F^- has an asymptotically vanishing imaginary part and thus does not contribute to $\Delta\sigma$, but only affects the behaviour of the real part ϱ of the elastic scattering amplitude in the forward direction (25a, 62). Recent analyses (61, 63) of ISR data on σ_{tot} and ϱ, however, leave little room for exotic contributions by such 'odderon' terms. Actually it can be proved (64) that $\Delta\sigma$ must go to zero, on the hypothesis that asymptotically Re F^- and Im F^- have the same sign (Fischer theorem). Measurements of ϱ indicate that this hypothesis is probably satisfied, despite the large errors, at ISR energies. Although, of course, one cannot exclude in principle that Re F^-/Im F^- changes sign at higher energy, it is reasonable to assume that the cross-section difference goes really to zero.

As a conclusion, the data seem to support a stronger picture than the one conjectured by the Pomeranchuk theorem, in the sense that not only the cross-section ratio tends to unity, but also the difference appears to tend to zero.

4.1.3 CORNILLE-MARTIN THEOREM Some effort was made to extend the validity of the Pomeranchuk theorem also to elastic scattering. It was first recognized (60b) that analyticity and unitarity imply that the ratio of the forward elastic differential cross-sections of particle and antiparticle should tend to unity for $s \to \infty$ (If ϱ tends to zero, this statement is equivalent to the Pomeranchuk theorem). Furthermore,

based on the positivity of the absorptive parts of the elastic amplitude 11, Cornille and Martin (65) have shown that the above property is valid for the whole diffraction peak, namely:

$$\frac{d\sigma}{dt}^{\bar{a}b}[s,t(s)] \Big/ \frac{d\sigma}{dt}^{ab}[s,t(s)] \to 1 \qquad 30.$$

for any smooth t(s) such that the ratio {dσ[s,0]/dt}/{dσ[s,t(s)]/dt} stays finite as $s \to \infty$. As a consequence, the ratio of the slopes of the diffraction peak in pp and $\bar{p}p$ elastic scattering must approach unity as energy increases: a persistent shrinking in pp elastic scattering must be accompanied by a similar shrinking in $\bar{p}p$. This picture is indeed supported by experimental data, as can be seen in Figures 4 and 5. In particular, the slope measurement at the SPS Collider indicates that also for $\bar{p}p$ scattering a shrinkage of the elastic diffraction peak sets in at a rate compatible with ln s.

The theorem extends naturally to the asymptotic equality of the total elastic cross-sections of particle and antiparticle: $\sigma_{el}(\bar{a}b)/\sigma_{el}(ab) \to 1$ for $s \to \infty$. This feature is in good agreement with the experimental data, as shown in Figure 13a.

Another important consequence of the Cornille-Martin theorem is that, if the dip of the pp elastic scattering around $-t \approx 1.4$ GeV^2 at ISR energies belongs to the diffraction peak, then a similar dip should be present also in $\bar{p}p$ scattering (provided that ISR energies can really be considered as asymptotic). Models (24) that predict a different dip in pp and $\bar{p}p$ elastic scattering have to apply to a non-asymptotic situation: when diffraction dominates, the pp and $\bar{p}p$ dips must behave in the same way for $s \to \infty$ (43, 61). The data shown in Figure 9b point to a significant difference in the large-t region, where a shoulder

seems to be favoured rather than a dip in $\bar{p}p$ scattering. However, the limited statistics does not allow to draw a definite conclusion, particularly when one realizes, as discussed in Section 2.1.3, that at these energies the $\bar{p}p$ dip may be partially filled by a higher value of ϱ.

4.1.4 MacDOWELL-MARTIN BOUND It has been shown by MacDowell and Martin (66) that the shape of the forward elastic peak must satisfy the following bound, based on unitarity (disregarding terms of order 1/s):

$$(d/dt)\ \ln\ [\mathrm{Im}\ F(t)]|_{t=0} \geq (1/36\pi)\sigma_{tot}^2/\sigma_{el}\ . \qquad 31.$$

If the real part of the elastic amplitude can be neglected, the inequality 31 gives a bound on the forward slope B of the elastic peak:

$$B \geq (1/18\pi)\sigma_{tot}^2/\sigma_{el}\ . \qquad 32.$$

Experimental data show that this bound is almost saturated (within $\approx$ 15%). This should not be surprising since the equality $B = (1/16\pi)\sigma_{tot}^2/\sigma_{el}$ holds for a purely imaginary exponential amplitude.

An interesting consequence of the bound 32, together with the requirement of analyticity of the scattering amplitude and the assumption of a qualitatively saturated Froissart bound, is the prediction of a non-uniform behaviour of the slope of the diffraction peak near the forward direction (61, 67). One should notice that, if $\sigma_{tot} \sim \ln^2 s$, then B must increase at least as $\ln^2 s$: since analyticity constrains B not to exceed a $\ln^2 s$ behaviour one can conclude that the forward slope B must go just like $\ln^2 s$. Experimental data up to present energies do not give a clear indication of a $\ln^2 s$ behaviour of the forward slope, which

still may be consistent with a linear increase with ln s (see Figure 5a). It must be clear, however, that if σ_{tot} continues to rise as $\ln^2 s$, at some finite energy the forward slope must start to increase faster than ln s in order to prevent a violation of inequality 32.

4.1.5 AUBERSON-KINOSHITA-MARTIN THEOREM From the hypothesis of a qualitatively saturated Froissart bound follows a remarkable property of the scattering amplitude. In fact, if asymptotically σ_{tot} grows like $\ln^2 s$, also $\sigma_{el} \sim \ln^2 s$ (58). By the optical theorem, $d\sigma/dt|_{t=0}$ increases like $\ln^4 s$, so that the width of the diffraction peak must shrink like $1/\ln^2 s$ (note that a weaker shrinkage is excluded since it would produce σ_{el} larger than σ_{tot} at sufficiently high energy). As a matter of fact, it has been shown (68) that with this limiting behaviour not only the width but also the whole shape of the diffraction peak is constrained to exhibit a scaling property. More rigorously, neglecting odd signature contributions, if $\sigma_{tot}/\ln^2 s \to$ const for $s \to \infty$, then

$$\text{Im } F(s,t)/\text{Im } F(s,0) \to \phi(\tau) \ , \quad \text{Re } F(s,t)/\text{Re } F(s,0) \to (d/d\tau)[\tau\phi(\tau)] \ , \tag{33.}$$

where $\tau = t \ln^2 s$ and $\phi(\tau)$ is an entire function of order 1/2, i.e. analytic in τ and bounded by $\exp(c\sqrt{|\tau|})$. In other words, if the Froissart bound is saturated, the diffraction amplitude F(s,t) asymptotically reduces to a function of a single scaling variable, proportional to $t\sigma_{tot}$. This is a useful result for applications in phenomenology, which leads to predictions on the asymptotic behaviour of diffraction scattering that can be compared with experimental data and can allow testing whether an asymptotic regime is already installed at present energies.

4.2 Scaling as an Asymptotic Property: Comparison with High-Energy Data

If one believes that a qualitative saturation of the Froissart bound is already effective at present energies, then Equations 33 allow one to write the elastic-scattering amplitude in terms of two input parameters, σ_{tot} and ϱ, that can be determined by experiment at each energy, and of a universal function $\phi(\tau)$ (69):

$$d\sigma/dt = (1/16\pi)\ \sigma_{tot}^2\ \{\phi^2(\tau) + \varrho^2[(d/d\tau)\tau\phi(\tau)]^2\}\ . \qquad 34.$$

This differential equation can be solved numerically for $\phi(\tau)$ if all other quantities ($d\sigma/dt$, σ_{tot}, ϱ) are accurately known at a given energy. At other energies, the elastic differential cross-section $d\sigma/dt$ can then be computed by inserting the measured values of σ_{tot} and ϱ. It can be noticed that Equation 34 exhibits the same scaling property as Equation 25, apart from the presence of the quantity ϱ that depends on s alone. If one considers, however, that the real part of the amplitude is much smaller than the imaginary part (at all values of t except of course in the region of the dip) the geometrical scaling hypothesis formulated on the basis of the ISR data (see Section 3.5) appears to be more than a phenomenological description of diffraction scattering at high energy: it comes out naturally as an asymptotic property, provided that the Froissart bound is saturated. Should this be the case, relations 25 to 27 would hold asymptotically in a model-independent way.

The scaling function $\phi(\tau)$ has been computed in Reference (70) by solving numerically Equation 34 at $\sqrt{s}$ = 53 GeV, where the most accurate data exist. The solution obtained for $\phi(\tau)$ is shown in Figure 19a. It goes through zero at the position of the dip, which is partially filled by the real part of the amplitude. Owing to this feature, the behaviour

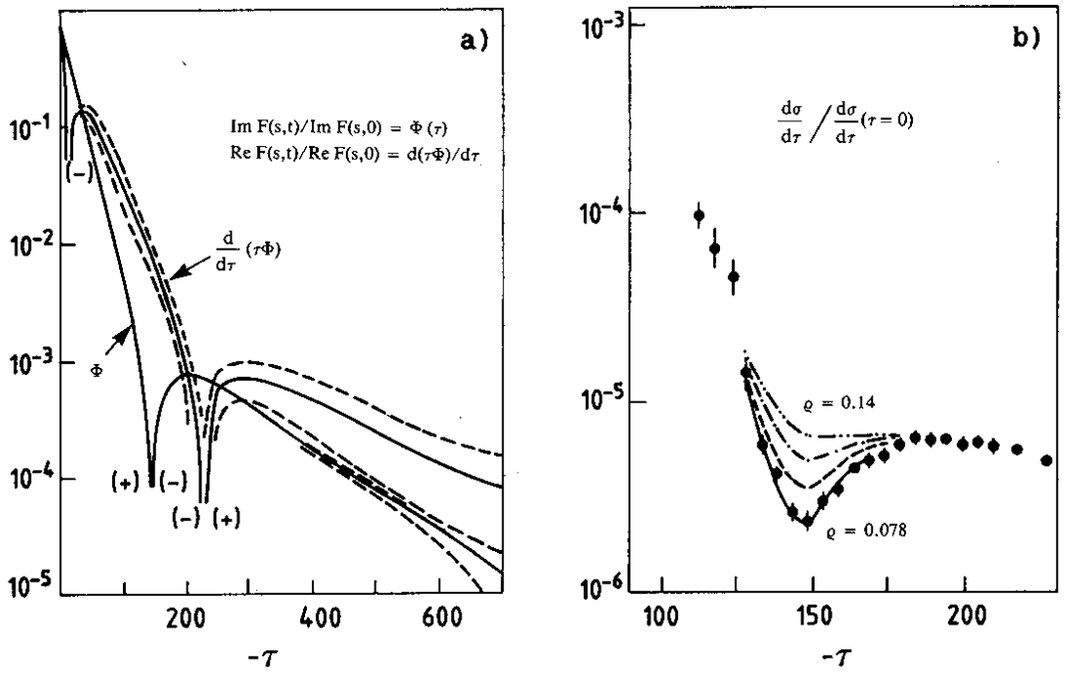

Figure 19. (a) The scaling function ♦ and its derivative computed by Equation 34 for pp elastic scattering at $\sqrt{s}$ = 53 GeV (the dashed lines represent the uncertainty of the calculation); (b) sensitivity of the dip-bump structure to the value of the real part ϱ (the four curves correspond to ϱ = 0.078, 0.10, 0.12, and 0.14, respectively) [from Reference (70)].

of dσ/dt at the dip is very sensitive to the real part ϱ in the forward direction, since Equation 34 states that the value of the cross-section becomes proportional to ϱ^2 where the imaginary part vanishes. This non-trivial connection between ϱ and the dip is illustrated in Figure 19b. The ISR data at the other energies are well reproduced by expression 34 also in the region of the dip, which is predicted to be deepest where ϱ is zero, and gradually filling in with increasing energy as the measured value of ϱ increases. The scaling violation at the dip, which appeared in the original geometrical hypothesis of Section 3.5, is therefore taken into account by the non-scaling term in Equation 34 due to the energy dependence of ϱ. At the energy of the SPS Collider, ϱ should attain a value high enough ($\varrho \geq 0.15$) to fill in completely the dip, which is expected to turn into a shoulder. Indeed recent data on $\bar{p}p$ elastic

scattering at $\sqrt{s}$ = 546 GeV (19) exhibit a shoulder at the predicted position. However, the measured value of the cross-section in this t-region is almost one order of magnitude higher than predicted (27), as shown in Figure 10b. This serious discrepancy is hard to reconcile. Furthermore, the rise of the ratios σ_{el}/σ_{tot} and σ_{tot}/B found at the Collider indicates that the nucleon opacity is increasing and provides clear evidence for violation of geometrical scaling. This growing behaviour is detailed in Figure 17, which illustrates the energy dependence of the inelastic overlap function from the ISR to the SPS Collider, obtained in the analysis (54) discussed in Section 3.5. In conclusion, the onset of an asymptotic geometrical scaling regime, which was believed to be effective already at the ISR, has to be pushed far beyond Collider energy, in spite of the observed $\sim \ln^2 s$ behaviour of σ_{tot} that had suggested a precocious saturation of the Froissart bound. This conflict with Equation 33 may raise a doubt as to whether the hypothesis of the Auberson-Kinoshita-Martin theorem is really verified; the present $\ln^2 s$ rise of σ_{tot} might only be a transient trend, different from the asymptotic behaviour.

4.3 Factorizing Eikonal Models

Another interesting approach stems from the original idea that was at the basis of the Chou-Yang model. In this geometrical picture, elastic scattering is considered as the result of the attenuation of the incoming wave through the extended distribution of matter inside the hadron (in close analogy with Glauber's optical model of hadron scattering on nuclei). In the pioneering works of Reference (71) the eikonal representation in impact parameter space (Equation 19) was

adopted with the assumption that the matter distribution G(b) is proportional to the charge distribution, i.e. the Fourier transform of the form factor. In subsequent works (72) after the discovery of rising cross-sections at the ISR, the energy dependence of σ_{tot} was taken into account by introducing a non-constant factor K(s) in the opaqueness: $\Omega(s,b) = K(s)G(b)$. At a given energy, the factor K is empirically determined by the value of σ_{tot} via Equation 15. Such a factorized form of the eikonal function allowed the generalization of the model, still preserving its original physical concept.

Already several years before the ISR results, on the other hand, Cheng and Wu (39) had deduced in the framework of massive QED that the asymptotic behaviour of the elastic amplitude should be of the eikonal kind with $K(s) \propto s^c$ (c is a positive constant) and G(b) decreasing exponentially at large b. It should be noticed that this result has a remarkable predictive power since it implies that the edge of the profile function 19 moves towards larger values of b proportionally to ln K(s), while its central part approaches the unitarity limit of 1/2 as the energy increases. The interacting hadron tends to appear as a black core whose radius grows as ln s surrounded by a grey fringe of constant width, and to behave just as in the limiting case discussed in Section 4.1.1, completely saturating the Froissart bound at infinite energy. This model therefore predicts that for all hadrons at extremely high energies the total cross-section grows as $\ln^2 s$, the elastic diffraction peak shrinks indefinitely, and the ratio σ_{el}/σ_{tot} rises with energy towards the limit 1/2. All these qualitative predictions seem indeed to be supported by experimental data. In order to improve the quantitative agreement with the data, the model was subsequently implemented (28) with various phenomenological parametrizations of the

hadronic-matter distribution G(b). Sometimes an expression of the kind $\exp [-\lambda(b^2 + b_0^2)^{1/2}]$ has been adopted (28a), which essentially is a Gaussian at small b with an exponential tail at $b >> b_0$, in close analogy with the behaviour of the Fourier transform of a dipole form factor $1/(1 - t/\mu^2)^2$. Other authors (28b) have tried to multiply a dipole form factor by an ad hoc slowly varying function of t. In all cases, good fits to the data are obtained, and the shoulder at large t in $\bar{p}p$ elastic scattering at the SPS Collider is predicted with about the correct height (see Figure 10b). Anyway, independently of a quantitative comparison of these specific parametrizations with experimental data, it is a fact that the qualitative predictions of the bare eikonal formulation of the original models have had remarkable confirmation, first by the $\sim \ln^2 s$ rise of the total cross-section found at the ISR, and now at the Collider by the further observation that the ratio σ_{el}/σ_{tot} also grows with energy.

5. CONCLUSIONS

The operation of the CERN ISR with protons and antiprotons has allowed the study of the expected similarity of the dominant features of particle and antiparticle in a new higher energy range. The observed convergence of the properties of pp and $\bar{p}p$ scattering reinforces the feeling that the first symptoms of an asymptotic regime do show up already at ISR energies.

The CERN SPS Collider has made accessible to experimentation an energy domain which is still one order of magnitude higher, making a long bound towards the land where the general principles prevail. In order to investigate the asymptotic features of hadron scattering, it is sensible to compare ISR pp data directly with Collider $\bar{p}p$ data, in so far as at

such energies the two reactions should exhibit practically the same behaviour.

In spite of the $\sim \ln^2 s$ growth of the total cross-section, the predicted asymptotic property of geometrical scaling is not observed in Collider $\bar{p}p$ data: the geometrical scaling behaviour found at the ISR should therefore be considered a merely transient feature. The apparent contradiction with the Auberson-Kinoshita-Martin theorem may lead one to question whether the σ_{tot} rise at this rate will really persist.

New light will be shed by the measurement of the real part ϱ at the SPS Collider, which is sensitive to the derivative of σ_{tot}. This will indicate the trend of the total cross-section beyond presently available energies, waiting for direct measurements at the forthcoming colliders. Should the $\sim \ln^2 s$ rise persist, the picture presented by the eikonal models could really be true: a steadily increasing opaqueness would lead all hadrons to reach the black disc limit at infinite energy. The Froissart bound would then tend to be quantitatively saturated very slowly with increasing energy. In this case the $\sim \ln^2 s$ dependence of σ_{tot} observed already at energies as low as those at the ISR should be interpreted as a precocious qualitative saturation of the Froissart bound, and would stay on more and more quantitatively at higher and higher energy. The hypothesis of the Auberson-Kinoshita-Martin theorem would actually be true asymptotically and geometrical scaling should indeed be regarded only as an asymptotic property.

Measurements at future big hadron colliders will be exciting and may eventually settle these tantalizing questions, making a further step towards the comprehension of the underlying dynamics.

ACKNOWLEDGEMENTS

It is a pleasure to thank all our colleagues of the UA4 Collaboration, and Professors G. Bellettini and A. Martin for useful discussions.

Literature Cited

1. Amaldi, U. et al. Phys. Lett. 44B:112-18 (1973)
2. Amendolia, S.R. et al. Phys. Lett. 44B:119-24 (1973); Nuovo Cimento 17A:735-55 (1973)
3. Möhl, D. et al. Phys. Rep. 58:73-119 (1980) and references therein
4a. Giffon, M., Predazzi, E. Riv. Nuovo Cimento 7 No. 5:1-62 (1984)
4b. Kamran, M. Phys. Rep. 108:275-399 (1984)
4c. Alberi, G., Goggi, G. Phys. Rep. 74:1-207 (1981)
4d. Fischer, J. Phys. Rep. 76:157-214 (1981)
4e. Giacomelli, G., Jacob, M. Phys. Rep. 55:1-132 (1979)
4f. Predazzi, E. Riv. Nuovo Cimento 2 No. 11:1-43 (1979); Riv. Nuovo Cimento 6:217-93 (1976)
4g. Amaldi, U., Jacob, M., Matthiae, G. Ann. Rev. Nucl. Sci. 26: 385-456 (1976)
4h. Giacomelli, G. Phys. Rep. 23:123-235 (1976)
4i. Roy, S. M. Phys. Rep. 5C:125-96 (1972)
4j. Block, M.M., Cahn, R.N. preprint LBL-17522, submitted to Rev. Mod. Phys.
5. Schubert, K. R. Tables on pp elastic scattering. In Landolt-Börnstein, New Series. Berlin: Springer-Verlag, vol. I/9a pp. 216-86 (1979), and references therein. See also Reference (42).

6. West, G. B., Yennie, D. R. Phys. Rev. 172:1413-22 (1968); Locher, M. P. Nucl. Phys. B 2:525-31 (1967); Cahn, R.N. Zeit. Phys. C15: 253 (1982)

7. Amaldi, U. et al. Phys. Lett. 66B:390-94 (1977)

8. Bartenev, V. et al. Phys. Rev. Lett. 31:1367-70 (1973)

9. Amos, N. et al. Phys. Lett. 120B:460-64 (1983); Phys. Lett. 128B:343-48 (1983)

10. Bronzan, J. B., Kane, G. L., Sukhatme, U. P. Phys. Lett. 49B: 272-76 (1974)

11. Sidhu, D. R., Sukhatme, U. P. Phys. Rev. D 11:1351-53 (1975)

12. Khuri, N. N., Kinoshita, T. Phys. Rev. 137:B720-29 (1965)

13a. Breakstone, A. et al. Nucl. Phys. B 248:253-60 (1984)

13b. Breakstone, A. et al. preprint CERN-EP/85-9 (1985), submitted to Phys. Rev. Lett.

14a. Burq, J. P. et al. Phys. Lett. 109B:124-28 (1982)

14b. Block, M.M., Cahn, R.N. Phys.Lett. 120B:229-32 (1983)

14c. Gauron, P., Nicolescu, B. Phys. Lett. 143B:253-58 (1984)

15. Schiz, A. et al. Phys. Rev. D 24:26-45 (1981); Ayres, D. S. et al. Phys. Rev. D 15: 3105-38 (1977); Akerlof, C. W. et al. Phys.Rev. D 14:2864-77 (1976)

16. Bozzo, M. et al. Phys. Lett. 147B:385-91 (1984)

17. Battiston, R. et al. Phys. Lett. 127B:472-75 (1983); Phys. Lett. 115B:333-37 (1982)

18. Arnison, G. et al. Phys. Lett. 128B:336-42 (1983)

19. Bozzo, M. et al. Int. Conf. on High Energy Physics, Brighton, 1983, paper 116; preprint CERN-EP/85-31 (1985), submitted to Phys. Lett. B

20. Matthiae, G. 15th Symposium on Multiparticle Dynamics, Lund, 1984

21. Nagy, E. et al. Nucl. Phys. B 150:221-67 (1979)

22. Asa'd, Z. et al. Phys. Lett. 108B:51-54 (1982); Phys. Lett. 128B: 124-28 (1983); Phys. Lett. 130B:335-39 (1983); preprint CERN-EP/84-144 (1984), submitted to Nucl. Phys. B

23. Rubinstein, R. et al. Phys. Rev. D 30:1413-31 (1984)

24. Donnachie, A., Landshoff, P. Nucl. Phys. B 231:189-204 (1984); Phys. Lett. 123B:345-48 (1983)

25a. Fukugita, M., Kwiecinsky, J. Phys. Lett. 83B:119-22 (1979)

25b. Martin, A. CERN-TH.4082/84 (1984)

26. Islam, M. M., Fearnley, T., Guillaud, J. P. Nuovo Cimento 81A:737 (1984)

27. Dias de Deus, J., Kroll, P. J. Phys. G 9:L81-84 (1983)

28a. Cheng, H., Walker, J. K., Wu, T. T. Phys. Lett. 44B:97-101 (1973)

28b. Bourrely, C., Soffer, J., Wu, T. T. Phys. Rev. D 19:3249-60 (1979): Nucl. Phys. B 247:15-28 (1984); preprint CPT 84/PE.1674 (1984)

28c. Chiu, C. Phys. Lett. 142B:309-14 (1984)

28d. Glauber, R. J., Velasco, J. Phys. Lett. 147B:380-84 (1984)

29. van der Meer, S. CERN Internal Report ISR-PO/68-31 (1968)

30. Rubbia, C. CERN $p\bar{p}$ NOTE 38 (1977)

31. Amendolia, S. R. et al. Proc. Int. Conf. on Instrumentation for High Energy Physics, Frascati, 1973. Frascati: Laboratori Nazionali del Comitato Nazionale per l'Energia Nucleare, pp. 397-401 (1973)

32. Bosser, J. et al. Internal Report CERN/SPS 84-11/DI-MST (1984), submitted to Nucl. Instrum. Methods

33. Amaldi, U. et al. Phys. Lett. 43B:231-36 (1973)

34. Amaldi, U. et al. Phys. Lett. 62B:460-66 (1976); Nucl. Phys. B 145:367-401 (1978)

35. Battiston, R. et al. Phys. Lett. 117B:126-30 (1982)

36. Bozzo, M. et al. Phys. Lett. 147B:392-98 (1984)

37. Yodh, G. B., Pal, T., Trefil, S. J. Phys. Rev. Lett. 28:1005-8 (1972)

38. Heisenberg, W. Kosmische Strahlung. Berlin: Springer-Verlag, pp. 148-64 (1953)

39. Cheng, H., Wu, T. T. Phys. Rev. Lett. 24:1456-60 (1970)

40a. Ambrosio, M. et al. Phys. Lett. 115B: 495-502 (1982)

40b. Carboni, G. et al. preprint CERN-EP/84-163 (1984), submitted to Nucl. Phys. B

41. Lukaszuk, L., Nicolescu, B. Lett. Nuovo Cimento 8:405-13 (1973); Kang, K., Nicolescu, B., Phys. Rev. D 11:2461-65 (1975); Gauron, P., Nicolescu, B., Phys. Lett. 124B:429-34 (1983)

42. Amaldi, U., Schubert, K. R. Nucl. Phys. B166:301-20 (1980)

43. Martin, A. Proc. 4th Topical Workshop on Proton-Antiproton Physics, Berne, 1984. CERN 84-09, pp. 308-13 (1984)

44. Baumel, J., Feingold, M., Moshe, M. Nucl. Phys. B 198:13-25 (1982); White, A. R., Fermilab preprint CONF 82/16-THY (1982); Baig, M., Bartels, J., Dash, J. W. Nucl. Phys. B 237:502-24 (1984)

45. Ter-Martirosyan, K. A. Paper submitted to the 22nd Int. Conf. on High Energy Physics, Leipzig, 1984 and references therein

46. Van Hove, L. Nuovo Cimento 28: 798-817 (1963); Rev. Mod. Phys. 36: 655-65 (1964)

47. Grein, W., Guigas, R., Kroll, P. Nucl. Phys. B 89:93-108 (1975); Kroll, P., Fortschr. Phys. 24:565 (1976)

48. Amaldi, U. Proc. 2nd Int. Conf. on Elementary Particles, Aix-en-Provence, 1973, published in J. Phys. (France) Suppl. 10: C1 241-59 (1973)

49. de Groot, E. H., Miettinen, H. I. Proc. 8th Rencontre de Moriond, Méribel-les-Allues, 1973. Orsay: Laboratoire de Physique Théorique et Particules Elémentaires, pp. 193-234 (1973)

50. Henyey, F. S., Hong Tuan, R., Kane, G. L. Nucl. Phys. B 70:445-60 (1974)

51. Henzi, R., Valin, P. Phys. Lett. 48B:119-24 (1974)

52. Miettinen, H. I. Proc. 9th Rencontre de Moriond, Méribel-les-Allues, 1974. Orsay: Laboratoire de Physique Théorique et Particules Elémentaires, pp. 363-402 (1974)

53. Henzi, R., Valin, P. Nucl. Phys. B 148:513-37 (1979)

54. Henzi, R., Valin, P. Phys. Lett. 132B:443-48 (1983); Phys. Lett. 149B: 239-44 (1984); paper submitted to the 22nd Int. Conf. on High Energy Physics, Leipzig, 1984; Henzi, R., Proc. 4th Topical Workshop on Proton-Antiproton Physics, Berne, 1984. CERN 84-09, pp. 314-21 (1984); Valin, P., Z. Phys. C 25:259-67 (1984)

55. Pomeranchuk, I. Ia. Zh. Eksp. Teor. Fiz. 34:725-28 (1958); Sov. Phys. JETP 7:499-501 (1958)

56. Froissart, M. Phys. Rev. 123: 1053-57 (1961)

57. Martin, A., Phys. Rev. 129:1432-36 (1963); Nuovo Cimento 42:930-54 (1966)

58a. Lukaszuk, L., Martin, A. Nuovo Cimento 52A:122-45 (1967)

58b. Martin, A. In A Discussion on pp Scattering at Very High Energies, London, 1973. Proc. R. Soc. London A 533:503-7 (1973)

59. Kupsch, J. Nuovo Cimento 71A:85-103 (1982)

60a. Eden, R. J. Phys. Rev. Lett. 16:39-41 (1966)

60b. Kinoshita, T. Phys. Rev. D 2:2346-48 (1970); in Perspectives in Modern Physics, ed. R. E. Marshak. New York: Wiley, pp. 211-13 (1966)

60c. Volkov, G. G. et al. Teor. Mat. Fiz. 4:196-201 (1970)
Truong, T. N., Lam, W. S. Phys. Rev. D 6:2875-83 (1972);
Grunberg, G., Truong, T. N. Phys. Rev. Lett. 31:63-66 (1973);
Phys. Rev. D 9:2874-93 (1974)

61. Martin, A. Z. Phys. C 15:185-91 (1982)

62. Joynson, E. et al. Nuovo Cimento 30A:345-84 (1975)

63. Block, M. M., Cahn, R. N. Phys. Lett. 120B:224-28 (1983)

64. Fischer, J., Saly, R., Vrkoc, I. Phys. Rev. D 18: 4271-81 (1978)

65. Cornille, H., Martin, A. Phys. Lett. 40B:671-74 (1972); Nucl. Phys. B 48: 104-16 (1972); Nucl. Phys. B 49:413-40 (1972); Nucl. Phys. B 77:141-62 (1974)

66. McDowell, S. W., Martin, A. Phys. Rev. 135:B960-62 (1964)

67. Martin, A., Proc. 3rd Topical Workshop on Proton-Antiproton Physics, Rome, 1983. CERN 83-04, pp. 351-71 (1983)

68. Auberson, G., Kinoshita, T., Martin, A. Phys. Rev. D 3:3185-94 (1971)

69. Martin, A. Lett. Nuovo Cimento 7:811-12 (1973)

70. Dias de Deus, J., Kroll, P. Acta Phys. Pol. B 9:157-65 (1978)

71. Wu, T. T., Yang, C. N., Phys. Rev. 137:B708-16 (1965); Byers, N., Yang, C. N. Phys. Rev. 142:976-81 (1966); Chou, T. T., Yang, C. N. Proc. 2nd Int. Conf. on High Energy Physics and Nuclear Structure, Rehovoth, 1967, ed. G. Alexander. Amsterdam: North Holland, pp. 348-59 (1967); Chou, T. T., Yang, C. N. Phys. Rev. 170:1591-96 (1968); Durand, L., Lipes, R. Phys. Rev. Lett. 20: 637-40 (1968)

72. Hayot, F., Sukhatme, U. P. Phys. Rev. D 10:2183-85 (1974)
Chou, T. T., Yang, C. N. Phys. Rev. D 19:3268-73 (1979)